PHILOSOPHICAL TRANSACTIONS OF THE ROYAL SOCIETY A

rsta.royalsocietypublishing.org

Review

Cite this article: Sleep NH, Zahnle KJ, Lupu RE. 2014 Terrestrial aftermath of the Moon-forming impact. *Phil. Trans. R. Soc. A* **372**: 20130172.
http://dx.doi.org/10.1098/rsta.2013.0172

One contribution of 19 to a Discussion Meeting Issue 'Origin of the Moon'.

Subject Areas:
geophysics, Solar System, astrobiology, atmospheric science, plate tectonics, geochemistry

Keywords:
Hadean, magma ocean, ^{142}Nd, runaway greenhouse, CO_2 subduction, planetary habitability

Author for correspondence:
Norman H. Sleep
e-mail: norm@stanford.edu

Terrestrial aftermath of the Moon-forming impact

Norman H. Sleep[1], Kevin J. Zahnle[2] and Roxana E. Lupu[2]

[1]Department of Geophysics, Stanford University, Stanford, CA 94305, USA
[2]NASA Ames Research Center, Moffett Field, CA 94035, USA

Much of the Earth's mantle was melted in the Moon-forming impact. Gases that were not partially soluble in the melt, such as water and CO_2, formed a thick, deep atmosphere surrounding the post-impact Earth. This atmosphere was opaque to thermal radiation, allowing heat to escape to space only at the runaway greenhouse threshold of approximately 100 W m^{-2}. The duration of this runaway greenhouse stage was limited to approximately 10 Myr by the internal energy and tidal heating, ending with a partially crystalline uppermost mantle and a solid deep mantle. At this point, the crust was able to cool efficiently and solidified at the surface. After the condensation of the water ocean, approximately 100 bar of CO_2 remained in the atmosphere, creating a solar-heated greenhouse, while the surface cooled to approximately 500 K. Almost all this CO_2 had to be sequestered by subduction into the mantle by 3.8 Ga, when the geological record indicates the presence of life and hence a habitable environment. The deep CO_2 sequestration into the mantle could be explained by a rapid subduction of the old oceanic crust, such that the top of the crust would remain cold and retain its CO_2. Kinematically, these episodes would be required to have both fast subduction (and hence seafloor spreading) and old crust. Hadean oceanic crust that formed from hot mantle would have been thicker than modern crust, and therefore only old crust underlain by cool mantle lithosphere could subduct. Once subduction started, the basaltic crust would turn into dense eclogite, increasing the rate of subduction. The rapid subduction would stop when the young partially frozen crust from the rapidly spreading ridge entered the subduction zone.

Royal Society Publishing

1. Introduction

A widely discussed hypothesis for the origin of the present Earth–Moon system involves the collision of a Mars-sized object with a Venus-size object (e.g. [1–3]). The immediate ballistic aftermath of the impact is beyond the scope of this paper. Our model assumes that the Earth can be described as a gravitationally stable body with a central core, with the Moon already condensed outwards of Roche's limit. During the time under consideration, the Earth's mantle cooled from a mostly molten state to a mostly solid state, as discussed in more detail by Lupu *et al*. [4]. Our paper expands on the previous work of Zahnle *et al*. [5].

The purpose of this paper is to examine the geodynamics of the cooling Earth, investigating the interplay between the interior, the surface and the atmosphere, and emphasizing the role played by tidal heating. Given the meagre Hadean geological record, we attempt to identify geochemical effects that may be preserved, allowing observation. We show that the heat flow from the Earth's interior could significantly affect its climate only for a period of about 10 Myr, after which the Earth probably settled into a warm solar-heated greenhouse of approximately 500 K with approximately 100 bar (10 MPa, 10^6 kg m^{-2}) of CO_2 in the atmosphere [6]. Finally, we pay attention to the demise of the massive CO_2 atmosphere and the emergence of the Earth as a habitable planet. We follow the evolution of the Earth in chronological order, concentrating on the effects due to the presence of the Moon. The Moon's evolution tidally coupled with the cooling Earth is beyond the scope of this paper. We refer the reader to the works of Solomatov [7] and Elkins-Tanton [8] for a general discussion of magma oceans, independent of the Moon.

2. Early atmospheric behaviour

In the initial stages, the climate of the molten Earth was dominated by internal heat. The rate at which the planet radiated heat to space was controlled by the infrared opacity of the atmosphere.

(a) Heat flux through earliest atmosphere

Following Lupu *et al*. [4], we take an initial atmospheric composition given by the gases in equilibrium with the magma ocean. The chemical equilibrium calculations (see also [9]) show that this atmosphere will be constituted mostly of water and CO_2. The total mass of the atmosphere is an input parameter in the model, and we fix it by choosing a total surface pressure (1000 bar) that allows a total water vapour mass in the atmosphere comparable to that of the present ocean.

The classical runaway greenhouse limit arises when the energy radiated by a planet is independent of the surface temperature, owing to the large opacity of the atmosphere. The atmosphere therefore traps the energy (solar, tidal or internal), and the surface heats up. As water is a strong radiation absorber, increasing the energy input into a water atmosphere leads to a powerful positive feedback loop until all water from the surface is vaporized. Changes in the atmospheric composition may break this chain, as the opacity of the atmosphere changes in this process. Today, an increase in the input heat flux (for example, from the Sun becoming more luminous over geological time) would result in a higher surface temperature and hence more water vapour in the atmosphere and a stronger greenhouse and a still higher surface temperature. Above the runaway greenhouse threshold, this amplification becomes unstable, and liquid water at the surface becomes impossible. The classical runaway greenhouse limit for a water atmosphere is approximately 300 W m^{-2} [10,11]. Recently, using more complete opacity data for hot H_2O, Goldblatt *et al*. [12] found 280 W m^{-2} for this limit. By vaporizing the current ocean volume, the surface could heat to more than 1500 K. With stronger opacity sources, it could become much hotter, and to current knowledge there is little to constrain the upper bound.

In the immediate aftermath of the Moon-forming impact, the lowermost atmosphere was in contact with the liquid mantle at the surface. NaCl, KCl and several sulfur-containing species like SO_2 are examples of geochemical volatiles that would have evaporated from the hot surface [4]. These vapour species along with water and CO_2 rendered the atmosphere opaque, with the

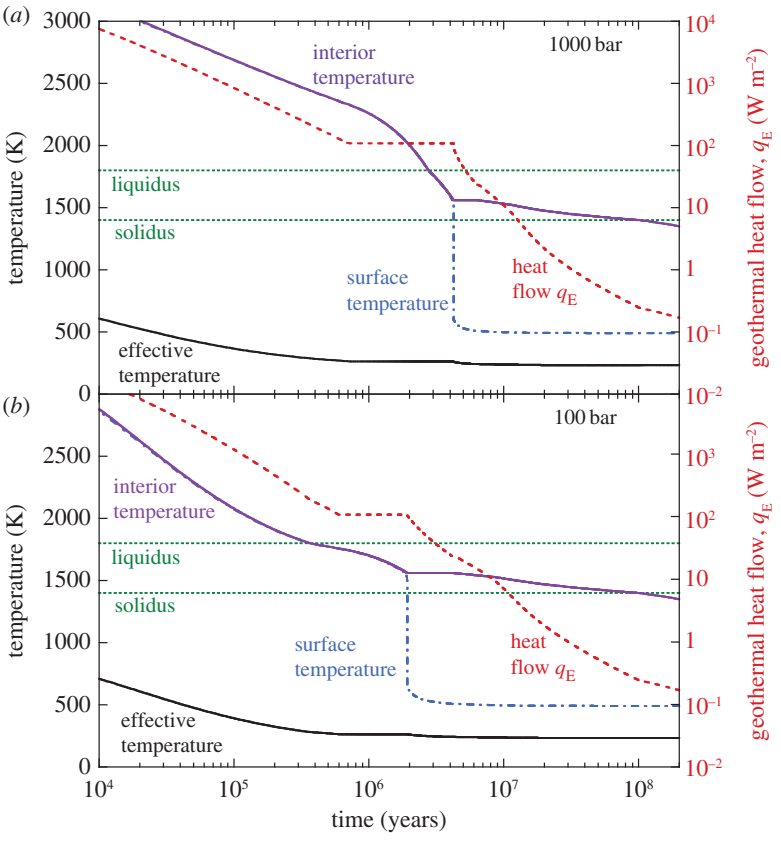

Figure 1. Thermal history of Earth's surface and interior computed using the code of Lupu *et al*. [4], for (*a*) 1000 bar (100 MPa) and (*b*) 100 bar (10 MPa) atmospheres in equilibrium with bulk silicate Earth (BSE) magmas. Heat flow (dashed) is plotted against the right-hand axis. Liquidus and solidus temperatures are indicated by horizontal dotted lines. The effective temperature approaches the runaway greenhouse threshold soon after the impact. The surface temperature is very close to the internal temperature until the mantle has partially frozen and a substantial thermal boundary layer forms. Tidal dissipation wanes at this time and the surface cools to a solar-dominated greenhouse. (Online version in colour.)

thermal radiation escaping at the runaway greenhouse threshold. The relationship between the radiating temperature at the top of the atmosphere and the surface temperature enables a simple estimate for the duration of the runaway greenhouse stage, as the surface proceeds to cool after the giant impact (e.g. [4,13–15]).

Figures 1 and 2 show the results of simple calculations using the combined internal and solar heat flows to illustrate the temperature evolution in the aftermath of the Moon-forming impact. The curves in figure 1 show the internal (mantle) temperature, surface temperature and effective radiating temperature of models under (*a*) 100 MPa and (*b*) 10 MPa BSE-equilibrated atmospheres. Figure 2 displays the relationship between the surface temperature of the planet and the effective temperature at the top of the atmosphere. This relationship has been derived from a set of radiative–convective equilibrium atmospheric models including the internal heat flow and the incoming solar radiation. Each model self-consistently computes the chemistry and energy balance [4].

For the solar luminosity in the early Hadean, we use the estimates of Claire *et al.* [16]. The Stefan–Boltzmann equation for a black body provides a way to express the energy radiated by an object in terms of an effective temperature. The radiative heat flow from the planet is given by

$$q_{\mathrm{rad}} = \sigma T_{\mathrm{rad}}^4, \tag{2.1}$$

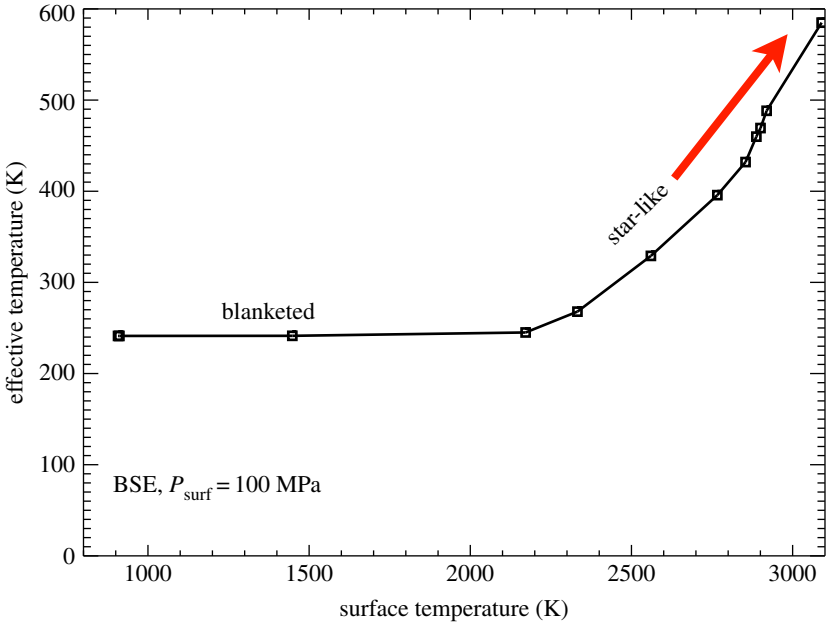

Figure 2. The effective temperature versus the surface temperature computed using the code of Lupu *et al*. [4] for a total pressure of 1000 bar (100 MPa). The surface magma ocean in equilibrium with the atmosphere has the composition of the BSE. The runaway greenhouse limit is reached below approximately 2200 K, in the 'blanketed' regime. At higher surface temperatures, the opacity of the atmosphere changes, and the effective temperature continues to increase with the surface temperature in a star-like fashion. (Online version in colour.)

where $\sigma = 5.67 \times 10^{-8}\,\mathrm{W\,m^{-2}\,K^{-4}}$ and T_{rad} is the effective radiating temperature of the object. In the absence of an atmosphere, the effective temperature is identical to the surface temperature (T_{surf}). Bare incandescent surfaces at magmatic temperatures (more than 1500 K) cool very rapidly to space. For example, the heat flow in (2.1) at 1500 K is $2.9 \times 10^{5}\,\mathrm{W\,m^{-2}}$. For the general case when an atmosphere surrounds the planet, it is traditional to express the observed or calculated heat flux from (2.1) by defining T_{rad} as the effective radiating temperature, even though the spectrum of the planet is not that of a black body.

The heat flow through the atmosphere q_{rad} is determined by both the globally averaged surface heat flow from the interior (q_{E}) and the solar heating. For example, the current atmosphere radiates at approximately 255 K so q_{rad} is approximately $240\,\mathrm{W\,m^{-2}}$. The Sun supplies essentially all this heat, because the globally averaged surface heat flow from the Earth's interior is only of the order of $0.1\,\mathrm{W\,m^{-2}}$. However, q_{E} had a major effect on climate after the giant impact, when it was a significant fraction of q_{rad}. Geothermal heat flow q_{E}, which includes tidal heating, is shown in figure 1 for the 100 MPa and 10 MPa atmospheres.

Roughly, we can estimate the Hadean q_{rad} in the absence of strong internal heat sources by assuming that the fraction of sunlight absorbed by the Hadean Earth was the same as today. If the radiative flux from the Sun in the Hadean was approximately 0.7 of the current value, then the fraction absorbed by the Hadean Earth would be $170\,\mathrm{W\,m^{-2}}$. The difference between this value and the classical runaway greenhouse limit ($280\,\mathrm{W\,m^{-2}}$) is $110\,\mathrm{W\,m^{-2}}$. This difference approximately demarcates a climate controlled by internal heat sources from a climate controlled by sunlight. For consistency, in the following example calculations, we will retain this value down to its insignificant digit. We will constrain the duration of the initial hot epoch by establishing scaling relationships for the behaviour of the atmosphere and the heat transport enabled by it.

(b) Initial atmospheric composition

Even though the Earth's back side would not have melted initially in the impact, the energy delivered was enough to render the Earth's mantle and surface mostly molten by the time that the Moon was formed (10^3–10^4 years). Our discussion starts with this stage as the initial condition. Water and CO_2 are only modestly soluble within molten rock of mantle composition at hundreds of bars pressure [17,18], and thus much of the global inventory of these materials entered the atmosphere [5,14,15,19]. This inventory would have been comparable to the modern inventory, since outer Solar System objects (comets) are unlikely to have added globally significant masses of water after the Moon-forming impact (e.g. [5,20]). The surface temperature of the Earth was probably around 2800 K, which corresponds to the surface temperature of mantle silicate on an adiabat in equilibrium with the fully molten mantle liquidus [21]. As the partial pressure for olivine (a proxy for the mantle) at approximately 3300 K is only 1 bar [22], and that for tektites (a proxy for continental crust (CC)) is only approximately 3 bar at 3350 K and 0.1 bar at 1640 K [23], silicates would have been minor atmospheric components.

Atmospheric compositions in equilibrium with likely rock types (CC and bulk silicate Earth (BSE)) have been calculated by Fegley & Schaefer [24] and Lupu *et al*. [4]. These works showed that important species contributing to the opacity of the atmosphere were metal and hydrogen halides, and sulfur compounds. For reference, the partial pressure of NaCl is approximately 0.01 bar at 1275 K [25], confining its vapour to the lower hot part of the atmosphere. In particular, SO_2 was predicted to produce strong spectral features, but its opacity is still only partially understood. In addition, pressure broadening and collision-induced absorption were important in the lower atmosphere, while atomic alkali opacity contributes in the upper regions. Also, at these exotic temperatures, molecules will contribute more opacity through the excitation of hot transitions that are not normally taken into account under the conditions of the present-day Earth. Overall, the atmosphere was opaque even if one ignores clouds in calculations [4].

3. Tidal dissipation within the nascent Earth

In the giant impact scenario, the Moon forms close to the Earth from the cloud of debris generated by the impact. The tidal coupling between the Earth and the Moon causes the conversion of the Earth's spin into the Moon's angular momentum, such that the Moon's orbit increases with time. At the same time, some of the tidal energy is dissipated in the Earth's magma ocean by eddy diffusion. Some variants of the impact hypothesis start with an Earth–Moon system with excess angular momentum (e.g. [26,27]), and thus require even more tidal dissipation inside the Earth. The energy released by this tidal braking goes into heating the Earth's interior.

The evolution of the Earth–Moon system after the Moon's accretion can be characterized in terms of two distinct phases. During the first phase, the Moon was close to the Earth, and the Earth's surface and mantle were almost completely molten. At this stage, the dissipation of tides was strong, but the rate of energy radiated to space was limited by the opacity of the atmosphere [4]. The energy dissipated by eddy diffusion was not strongly dependent on the interior temperature. Earth's atmosphere self-organized (in analogy to a star) and radiated the available heat production at an effective temperature of at most approximately 600 K (figure 1), if the total surface pressure was 1000 bar. This first phase lasts approximately 10^7 years, and the atmosphere progressively enters the runaway greenhouse regime as the surface temperature cools to below approximately 2000 K. During the second phase, the Moon was far enough away that the partially frozen material in the deep mantle dissipated tidal energy at a lower rate (figure 2). Heat escaped from the top of the atmosphere at the greenhouse threshold where the radiating temperature was approximately 240 K (see figure 2).

(a) Mechanics of tidal dissipation

The connection between tidal heating and the upper bound on radiative cooling created a stable climate buffer [4,5]. Dissipation by oscillating tidal stresses for hot silicate interiors can be characterized by the Maxwell time η/Γ (where η is viscosity and Γ is shear modulus). This dissipation is strongest when the Maxwell time is close to the tidal period. This time increased from its initial value of approximately 10^4 s (3 h) by a factor of a few as the Moon retreated and the lengths of the day and the month increased.

A material with a Maxwell time of the order of several hours (if cool) would resemble freshly accumulated muddy sediment. It would appear to be elastic on the time scale to safely walk across it but heavy objects would sink in over time. Petrologists call this mantle *partially crystalline mush*. We consider that water–rock mixtures in sediments provide a mechanical analogy for the shear modulus of magma–crystal mixtures, because the latter depends mainly on grain lattice size rather than on the properties of the fluid. The shear modulus of sediments is much lower than that of solid rock. For example, Magistrale *et al*. [28] and Hayashi *et al*. [29] compiled shear wave (S-wave) velocities β of sediments within Greater Los Angeles. The properties of the uppermost of these sediments represent the minimum shear modulus of a material that has compacted under gravity. They found an S-wave velocity of approximately 150 m s^{-1} at a density ρ of approximately 2000 kg m^{-2}. Applying $\Gamma = \rho\beta^2$ yields a shear modulus of 0.045×10^9 Pa. The corresponding viscosity for a Maxwell time of 10^4 s is then 4.5×10^{11} Pa s, which is appropriate for mush.

Significant tidal dissipation occurred even without having the precise combination of viscosity and shear modulus for which the Maxwell time matches the orbital time. First, the structure of the grain lattice in the mush affects both shear modulus and viscosity. Both quantities increase by progressive cooling and freezing. As such, the Maxwell time varies more slowly with melt fraction than it would if only viscosity was considered. Below we compare the viscosity and the Maxwell time for various scenarios.

For accumulated sediments that are buried to approximately 100 m depth, typical values of the S-wave velocity and density are 700 m s^{-1} and 2300 kg m^{-3} [28,29], respectively. For these values, the shear modulus is 10^9 Pa and the implied viscosity is 10^{13} Pa s.

The viscosity of hot rising plume material provides some analogy to the viscosity of barely frozen material on the nascent Earth. This parameter is not precisely constrained. For reference, Agrusta *et al*. [30] used 0.7×10^{18} Pa s in their models. Taking a value of approximately 70×10^9 Pa [31, table A3] for the mantle shear modulus, the Maxwell time becomes 10^7 s.

At the low-viscosity end, we consider slurries, which designate a material that could pass through a water main pipe if cool. As described in §4*c*, we can calculate the viscosity of a convecting slurry to be 2×10^9 Pa s, which implies a shear modulus of 2×10^5 Pa for a Maxwell time of 10^4 s. This value for the shear modulus is too low, and thus the Maxwell model is unlikely to represent slurry.

In addition, the work of Lamb [32] and the analogy with shallow sediments show that, in mixtures of solids and liquids, the dissipation of strain energy occurs over a broad frequency range, rather than a narrow one implied by the Maxwell model. The dissipation can be quantified in terms of $1/Q_S$, where Q_S is the quality factor for shear waves (an oscillation damps over Q_S oscillations). Values for Q_S for the shallow subsurface in California range from 30 [33] to 57–300 [34]. The nearly frozen domains within the nascent Earth can be thought of as analogous to the asthenosphere of modern Earth. In this case, the apparent Q is approximately 300 [31, pp. 368–369].

Overall, the Maxwell model can give a good approximation for the properties of a mush under the strongest tidal dissipation. However, significant tidal dissipation should occur in any partially molten material where the crystals mechanically interact with each other. A more sophisticated model for dissipation within mush and slurries would probably involve nonlinear interaction between tidal and convection stresses and is beyond the scope of this paper.

(b) Quasi-steady-state approach via tidal dissipation

We qualitatively follow tidal dissipation from the immediate aftermath of the Moon-forming impact until a quasi-stable balance between tidal heating and escape of heat near the runaway greenhouse threshold was achieved. Numerical models show that the impact heterogeneously heated the mantle (e.g. [1,2]). Cooler solid domain presumably sank downwards and ponded in the deep mantle, similar to modern slabs. It is likely that at this time shear strain heating occurred, the mantle was hot, and cooler regions were either near to or above the solidus. From §3*a*, it is apparent that some dissipation could have heated the cooler domains. The impact models predict a hot core that would have heated the cooler deepest mantle via stagnant-lid convection, as described in §4*a*. However, our formalism does not attempt to estimate the vigour of this process in the lowermost mantle.

The tidal-heating process within the cool mantle domains was probably unstable. If the global heating rate (insolation plus tides) was greater than the energy escape rate at the runaway greenhouse threshold (shown in figures 1 and 2), then the partially molten regions melted further, decreasing the global dissipation rate. Increasing the melt fraction reduced the viscosity of the material towards the optimum of approximately 4.5×10^{11} Pa s for dissipation. The process stabilized once the partially molten material within the mantle reached the amount needed to dissipate tides at the rate at which the heat could escape through the atmosphere.

This negative feedback loop leading to a stable state where the global heat flux remained near the runaway greenhouse threshold probably persisted as the Moon retreated from the Earth. This conveys the picture of a secularly cooling planet with a mantle that is almost, but not entirely, molten. We can assume that near the base of the mantle there was a layer of partially crystalline material with a viscosity of approximately 4.5×10^{11} Pa s, favourable for tidal dissipation, which occurred predominantly within this restricted layer. The rest of the mantle had very low viscosity and therefore was weakly heated. Heat from the dissipative layer was carried upwards by convection, at a rate set by the radiative cooling limit of the runaway greenhouse. If tidal heating in the layer exceeded this limit, then some of the partially molten dissipative mush was remelted, which in turn reduced tidal dissipation. What we have described is a negative (stabilizing) feedback that kept the total amount of tidal dissipation (and thus the total volume of non-melted material in the mantle) equal to the net rate at which the energy is radiated by the atmosphere to space. As the Moon receded from the Earth, tidal forcing weakened and the volume and thickness of the dissipating layer increased, in spite of negative feedback. This continued until the volume of the dissipating layer reached a maximum, filling either the mantle as a whole or just a depth range determined by the melting behaviour of silicates at high pressures.

The liquidus and solidus are generally thought to increase with depth more rapidly than the adiabat curve in the Earth's mantle [21] (cf. [35]). Thus, ignoring the heating from the core, we can assume that the mantle froze from the bottom up as it cooled (figure 3). Thus, the layer of partial melting and tidal dissipation moved upwards over time. The solid mantle beneath the dissipation zone and the liquid mantle above it could not significantly dissipate tides. The depth range over which dissipation occurred may have increased as the Moon retreated, keeping the global dissipation rate constant.

4. Physics of convection within the nascent Earth

We examine the thermal state of the Earth and show that it was largely solidified when the internal heat flow ceased to dominate climate. The Earth's molten interior convected vigorously. Conduction carried heat from the interior into the base of the atmosphere through a thin thermal boundary layer. The negative buoyancy of foundering parts of the boundary layer drove convection. We therefore apply the well-known construct of boundary-layer theory to constrain the heat flow from convection. This theory is applicable because the boundary layer was thin compared with the convecting region (e.g. [36–38]).

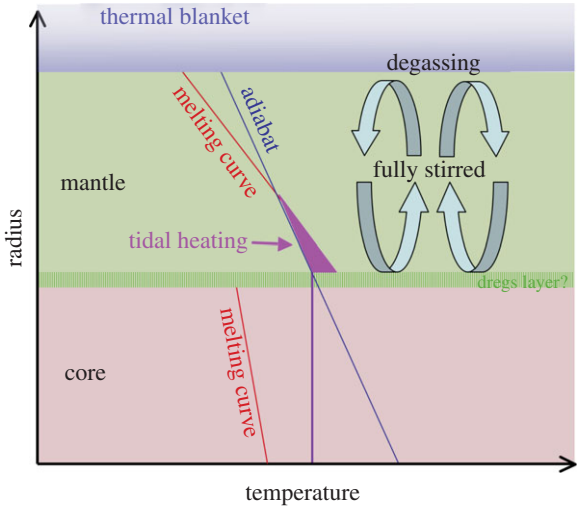

Figure 3. Schematic diagram of nearly molten magma ocean. Tidal heating occurred within partially crystalline material deep in the mantle. A layer of dense dregs may have accumulated deep in the mantle. (Online version in colour.)

(a) Scaling relationships for the convective heat flow

We present basic scaling relationships for the thickness of the boundary layer, its rate of sinking and the convective heat flow, following Sleep [39]. In this regard, we examine when the chemical reactions between the boundary layer and the atmosphere could first generate persistent compositional variations at the surface. Such reactions were initially unimportant. We show in this section that at first the thermal boundary was so thin and the temperature contrast across it so small that chemical equilibrium with the major volatile components of the atmosphere is reasonable (as assumed in figures 1 and 2). Furthermore, each batch of mantle material passed through the boundary layer hundreds of times. In this case, water and CO_2 concentrations in the mantle would have been saturated at a level where bubbles barely started to form at the liquid surface.

Simple scaling relationships for the heat transfer are useful to illustrate the basic properties of the thermal boundary layer. The fact that the heat flow for the Hadean runaway greenhouse threshold is known, approximately $110\,\mathrm{W\,m^{-2}}$, allows us to put these relationships in a simple form. The convective heat flow from the boundary layer equals the conductive heat flow through the boundary layer,

$$q_\mathrm{v} = q_\mathrm{cond} = k\frac{\Delta T_\mathrm{BL}}{\Delta Z_\mathrm{BL}}, \tag{4.1}$$

where $k \approx 2.5\,\mathrm{W\,m^{-1}\,K^{-1}}$ is the thermal conductivity, ΔZ_BL is the thickness of the boundary layer and ΔT_BL is the temperature contrast. The time scale for the boundary layer to cool (i.e. how long it stays at the surface before it returns to the interior of the convecting fluid) is

$$t_\mathrm{BL} = \frac{\Delta Z_\mathrm{BL}^2}{\kappa} = \frac{\rho C k \Delta T_\mathrm{BL}^2}{q_\mathrm{cond}^2}, \tag{4.2}$$

where $\kappa \equiv k/\rho\,C$ is the thermal diffusivity, ρ (here approximately $3300\,\mathrm{kg\,m^{-3}}$) is density and C (here approximately $1.25 \times 10^3\,\mathrm{J\,m^{-3}\,K^{-1}}$, [40]) is the specific heat per unit mass (essentially at constant pressure). For use later in the derivation, the scale velocity of the upward flow, $V_\mathrm{s} \equiv \Delta Z_\mathrm{BL}/t_\mathrm{BL}$, is equivalent to $\kappa/\Delta Z_\mathrm{BL}$.

We constrain the vigour of convection, the convective velocity and the heat flow by balancing forces within the boundary layer. We consider the force balance at the place where the boundary layer founders into the interior (subducts). The density difference between the boundary layer

and the interior scales with the temperature contrast ΔT_{BL}, that is $\Delta\rho = \rho\alpha\Delta T_{\mathrm{BL}}$, where α is the volume thermal expansion coefficient. The variations of stress within the thermal boundary layer scale with the lithostatic stress difference over a column of thickness ΔZ_{BL} as

$$\tau \approx \rho g \alpha \Delta T_{\mathrm{BL}} \Delta Z_{\mathrm{BL}}, \tag{4.3}$$

where g is the gravitational acceleration. We obtain the convection velocity by dimensionally integrating the strain rate over the thickness of the boundary layer. The strain rate is

$$\dot{\varepsilon} \approx \frac{V_{\mathrm{s}}}{\Delta Z_{\mathrm{BL}}} \approx \frac{\tau}{\eta}, \tag{4.4}$$

where η is the effective viscosity. Using the scaling relationship $V_{\mathrm{s}} \approx \kappa/\Delta Z_{\mathrm{BL}}$ and substituting for τ yields

$$\frac{\kappa}{\Delta Z_{\mathrm{BL}}} \approx \frac{\rho g \alpha \Delta T_{\mathrm{BL}} \Delta Z_{\mathrm{BL}}^2}{\eta}. \tag{4.5}$$

Solving for the convective heat flow in (4.1) yields the usual parametrized convection equation,

$$q_{\mathrm{v}} = Ak\Delta T_{\mathrm{BL}} \left[\frac{\rho g \alpha \Delta T_{\mathrm{BL}}}{\kappa \eta}\right]^{1/3} = Ak\Delta T_{\mathrm{BL}} \left[\frac{\rho g \alpha \rho C \Delta T_{\mathrm{BL}}}{k\eta}\right]^{1/3}, \tag{4.6}$$

where the bracket to the 1/3 power is dimensionally the inverse of the thickness of the thermal boundary layer $\Delta Z_{\mathrm{BL}}^{-1}$ (from equation (4.5)) and A is a constant of the order of 1 that depends on the upper boundary condition and whether the fluid is turbulent [7,36,37,41–43].

It is convenient to rewrite (4.6) in terms of the physical property T_η, the temperature needed to change viscosity by a factor of e (approx. 100 K). Observations of lava lakes and laboratory experiments on their analogues provide some insight into the proportionality relationship between ΔT_{BL} and T_η [41–43], as do numerical calculations [37]. That is, the temperature contrast across the actively flowing rheological boundary layer is aT_η. The empirical constant a for stagnant-lid convection is between 2.3 and 2.4 for a linear fluid. Viscosity then varies by a factor of approximately 10 within the rheological boundary layer.

Substituting T_η for ΔT_{BL} yields a well-known form of (4.6),

$$q_{\mathrm{v}} = A_{\mathrm{SL}} k T_\eta \left[\frac{\rho g \alpha T_\eta}{\kappa \eta}\right]^{1/3}, \tag{4.7}$$

where the multiplicative constant for a stagnant lithospheric lid is $A_{\mathrm{SL}} \approx 0.47$ [41–43]. The dimensionless constant for stagnant-lid convection A_{SL} now incorporates the constants A and a. The constant A_{FS} is approximately 1 for convection beneath a free surface [44], that is the hot atmosphere above the magma ocean.

(b) Qualitative thermal history

We use (4.6) and (4.7), noting that the viscosity of the Earth's interior varied by approximately 20 orders of magnitude as the magma ocean evolved from liquid to solid. Viscosity is thus the dominant parameter in (4.6) and (4.7), even though it is raised only to the 1/3 power. For our present purposes, there are three domains for equations (4.6) and (4.7). We follow the chronological order for the magma ocean in figure 1. (i) At first, the viscosity of the liquid magma was quite low. The stagnant-lid heat flow implied by (4.7) in this case was much greater than the runaway greenhouse threshold of approximately 110 W m^{-2}. The temperature contrast across the boundary layer in (4.6) then self-organized to a value much less than T_η, so that the heat flow was limited to approximately 110 W m^{-2}, the maximum allowed by the atmosphere. The viscosity contrast across the boundary layer was also small, as shown in §4*d*. That is, the flow behaved as isoviscous convection. (ii) The mantle cooled until the viscosity of the shallow fluid in (4.7) implied a heat flow of 110 W m^{-2}. Further cooling of the mantle increased the viscosity beyond the

point where the stagnant-lid heat flow in (4.7) could maintain the runaway greenhouse. We apply (4.7) later in the next subsection to estimate conditions at this transition. (iii) A significant cool solid lid formed beneath the warm atmosphere. Stagnant-lid convection is a feasible mode of heat transfer under this lid, but only at levels much smaller than $110\,\mathrm{W\,m^{-2}}$. For modern subduction, the full temperature contrast across a solid boundary layer drives solid-state convection. We discuss the initiation of plate tectonics in §6.

(c) Slurry convection at the end of the runaway greenhouse

A significant thermal boundary layer develops once the shallow mantle is partly crystalline (figure 1). We model the transition from isoviscous convection to stagnant-lid convection at this time using scaling relationships.

To apply (4.7), we need to distinguish among the parameters for liquid magma, mush and solid mantle. To the first order, viscosity decreases exponentially with temperature; the viscosity of liquid mantle is then formally

$$\eta_{\mathrm{liq}} = \eta_{\mathrm{L}} \exp\left[\frac{-(T - T_{\mathrm{ref}})}{T_{\eta\mathrm{L}}}\right], \tag{4.8}$$

where η_{L} is the viscosity at the reference temperature T_{ref} and $T_{\eta\mathrm{L}}$ is the scale temperature for a factor of e viscosity change in liquid magma, that is T_η in (4.7). The term $\eta_{\mathrm{L}} \exp(T_{\mathrm{ref}}/T_{\eta\mathrm{L}})$ is effectively one multiplicative constant. The reference temperature may be chosen for convenience. The viscosity of the solid mantle is analogously

$$\eta_{\mathrm{sol}} = \eta_{\mathrm{S}} \exp\left[\frac{-(T - T_{\mathrm{ref}})}{T_{\eta\mathrm{S}}}\right], \tag{4.9}$$

where η_{S} is the viscosity at the reference temperature and $T_{\eta\mathrm{S}}$ is the scale temperature for the solid, that is also T_η in (4.7).

The relevant parameters for applying (4.7) to liquid and solid convection are adequately constrained by available data to illustrate magma ocean properties. Scale temperatures from $T_{\eta\mathrm{L}} \approx T_{\eta\mathrm{S}} \approx 43\,\mathrm{K}$ to $T_{\eta\mathrm{L}} \approx T_{\eta\mathrm{S}} \approx 100\,\mathrm{K}$ have been widely used in the geodynamics literature. It suffices that the viscosity of fully molten mantle is quite low at shallow depths. Shaw [45] provides a formalism for computing this viscosity. For example, Stockstill-Cahill [46] computed $0.02\,\mathrm{Pa\,s}$ at 1950 K liquidus for mercurian peridotitic komatiite. Solomatov [38] assumed $0.1\,\mathrm{Pa\,s}$ in his calculations. We will assume that $\eta_{\mathrm{liq}} = 0.01\,\mathrm{Pa\,s}$. The values of the other parameters in (4.7) are well constrained and apply to both liquid and solid mantle; we let ρ be $3300\,\mathrm{kg\,m^{-3}}$; k be $2.5\,\mathrm{W\,m^{-1}\,K^{-1}}$; C be $1.25 \times 10^3\,\mathrm{J\,kg^{-1}\,K^{-1}}$; g be $9.8\,\mathrm{m\,s^{-2}}$; and α be $3 \times 10^{-5}\,\mathrm{K^{-1}}$.

By applying (4.7), we show that the shallow mantle was partly solid at the time of the transition to a heat flow of $110\,\mathrm{W\,m^{-2}}$. We let the scale temperature for mush be $T_{\eta\mathrm{M}} = 100\,\mathrm{K}$. The predicted viscosity in (4.7) (beneath a free surface with A_{FS} approximately 1, as for laminar flow, [44]) is $1.9 \times 10^9\,\mathrm{Pa\,s}$, which is appropriate for a partially molten slurry. The viscosity might decrease rapidly with temperature within partially molten mantle slurry. As seen from (4.6), the computed viscosity scales as $T_{\eta\mathrm{M}}^4$. To provide a range for the viscosity drop, at $T_{\eta\mathrm{M}} = 40\,\mathrm{K}$ the viscosity is $4.7 \times 10^6\,\mathrm{Pa\,s}$.

However, slurry with the computed range of viscosities is likely to have complicated properties. Like sediments and cumulates within magma chambers, the slurry will tend to compact under gravity, expelling melt. There is also a tendency for molten magma to intrude into partially molten slurry and into solids above it. The magma can also surround and isolate blocks of slurry and overlying solid. The surrounding blocks then may founder into the slurry. These processes increase the effective value for the temperature contrast between the sinking material and the hot fluid that drives convection, that is ΔT_{BL} in (4.6). For example, increasing the boundary temperature contrast to 400 K to account for foundering, and leaving the other parameters fixed, would increase the computed viscosity to $4.5 \times 10^{11}\,\mathrm{Pa\,s}$, which is the value we

obtained for a tidal Maxwell time of 10^4 s. In this case, the latent heat of freezing increases the effective value of the heat capacity and the increase of density upon freezing also increases the effective value of the thermal expansion coefficient.

Qualitatively, the convecting material was partially molten at the end of the runaway greenhouse epoch. The transition from liquid to solid viscosity occurred when the fraction of crystals became high enough that they needed to deform for flow to occur. Lupu *et al*. [4] applied these inferences in their calculations to parametrize the effect of crystal formation when the convecting interior was partly solid.

(d) Fully molten mantle convection

We continue by deriving the thickness of the boundary layer during the time when the runaway greenhouse controlled the heat flux, $q_v \approx 110\,\mathrm{W\,m^{-2}}$, through a fully liquid mantle. The appropriate multiplicative constant A in (4.7) for convection beneath a free surface (here, the atmosphere) is approximately 0.089 if we assume that the convection is mildly turbulent [38]. We retain $T_{\eta L}$ to be 100 K and round η_{liq} to the value of 0.01 Pa s. The predicted heat flow q_v in (4.1) for mildly turbulent flow is then $5.6 \times 10^4\,\mathrm{W\,m^{-2}}$. This value greatly exceeds the atmosphere limit of $q = 110\,\mathrm{W\,m^{-2}}$. The actual temperature contrast in (4.7) scales as $(q/q_v)^{3/4}$, giving a mere value of approximately 0.9 K. In this analysis, the boundary layer was just approximately 0.02 m thick. The computation supports the inference that the atmosphere maintained chemical equilibrium with the fluid mantle.

On the other hand, a 2 cm boundary layer may be too thin to be credible. First, the presence of any buoyant surface scum and foam acted as a blanket. For our parameters, a temperature drop of 44 K would occur across each metre of scum. We do not have a good way to constrain the physical and chemical properties of scum and foam.

(e) Duration of the molten mantle

We can estimate the duration of the geothermally supported runaway greenhouse state of the Earth. Internal heat sources could have been climatically significant only for the modest geological time of approximately 10 Myr (figure 1). We provide a simple calculation drawing on the result that shallow regions were partially molten at the end of this epoch. The available heat per surface area for a temperature change of ΔT_{man} throughout the mantle is

$$Q = \frac{C M_{man}}{4\pi R^2}\Delta T_{man}, \tag{4.10}$$

where $M_{man} = 4 \times 10^{24}$ kg is the mass of the mantle and R is the radius of the Earth. The heat capacity C of solid silicates is approximately $1.25\,\mathrm{kJ\,kg^{-1}\,K^{-1}}$. That is, cooling of the mantle at a rate of $3.2\,\mathrm{K\,Myr^{-1}}$ produces $1\,\mathrm{W\,m^{-2}}$ of surface heat flow. We ignore core cooling, as we do not know its rate relative to the mantle on the Hadean Earth and as we are striving for factor-of-2 precision in computed cooling times from such scaling relationships.

The critical heat flow of $110\,\mathrm{W\,m^{-2}}$ would cool the mantle at a rate of approximately $300\,\mathrm{K\,Myr^{-1}}$, ignoring latent heat. The effect of latent heat is equivalent to a cooling of a few hundred kelvins [47], as in the models of Lupu *et al*. [4]. In addition, tidal heating prolonged the molten epoch by a factor of approximately 2–4 [4] (figure 1). Their more sophisticated calculations indicate that climatically significant internal heat flow lasted approximately 10 Myr. The thermal histories of Elkins-Tanton [19] and Hamano *et al*. [15] have modestly smaller cooling times, partly because less total heat had to escape. Any epoch of high heat flow after the transition from the runaway greenhouse was geologically brief. For example, a heat flow of $10\,\mathrm{W\,m^{-2}}$ would have cooled the mantle by 320 K in 10 Myr.

A similar calculation does not work for ancient Venus, for which the difference between insolation and the runaway greenhouse limit was small and geothermal heat flows of the order of $10\,\mathrm{W\,m^{-2}}$ held the fate of the planet in the balance [15].

(f) Cycle time of the mantle

With regard to chemical equilibrium between the molten mantle and the atmosphere, the computed thickness of the thermal boundary layer is quite thin. Furthermore, material is cycled through the boundary layer hundreds of times, because the cooling on each pass through the boundary layer is only $\Delta T_{\mathrm{BL}} \approx 0.9\,\mathrm{K}$ on each trip. The number of times a parcel cycles through the boundary layer for a given cooling of the whole mantle equal to ΔT_{man} is

$$N_{\mathrm{cycle}} \approx \frac{\Delta T_{\mathrm{man}}}{\Delta T_{\mathrm{BL}}}. \tag{4.11}$$

The mantle cooled several hundred kelvins until the surface froze, indicating that material cycled through the boundary layer hundreds of times.

Geothermal heat available for the remainder of the Hadean is modest. The mantle had already cooled to the point where partially molten slurry existed near its surface. In terms of (4.10), the internal temperature change during the slurry epoch is comparable to the temperature change in the boundary layer (figure 1), so the mantle would have circulated through slurry about once. Furthermore, most of the mantle was probably already frozen on the adiabat of the slurry epoch. Only modest cooling (at most a few hundred kelvins) of the mantle on average is allowed between approximately 10 Myr after the Moon-forming impact and the approximately 3.8 Ga age in the Archaean for which petrologists are able to infer mantle temperatures by studying komatiite lavas [48,49]. The hottest Archaean komatiites were probably the product of mantle plumes, indicating that Archaean mantle temperatures were heterogeneous. The fraction of partial melting within Archaean plumes was up to approximately 50% mantle [50], enough to form slurry if globally present.

Hadean convection could have been sluggish after the transition despite greater amounts of radioactivity. The equivalent heat flux per unit area was of the order of $0.1\,\mathrm{W\,m^{-2}}$ [49], modestly higher than the present global mantle heat flow of approximately $0.07\,\mathrm{W\,m^{-2}}$. Herzberg *et al.* [49] prefer a mantle thermal history where the internal temperature at the end of vigorous initial Hadean convection was 50–150 K hotter than present. The internal temperature then increased to a maximum of 150–250 K hotter than present at around 3 Ga. Globally averaged tectonic rates would have been slower than present ones during this Hadean and Archaean epoch.

5. Geochemical fractionation

Figure 1 indicates that the mantle was mostly solid at the end of the internally heated runaway greenhouse. The internally heated runaway greenhouse and any epoch of very vigorous convection following it were geologically brief. We use analogies to current processes and simple physics to illustrate situations during these epochs that may have left durable geochemical tracks within extant rocks. In particular, a tracer would be partial crystallization that fractionated elements between crystals and melts.

(a) Shallow geochemical processes

As already noted, the liquidus and solidus of the upper mantle are steeper than the adiabatic gradient (figure 3). Familiar processes, including those beneath modern mid-oceanic ridges, provide an analogy for this case. Ascending solid material partially melted, while dense crystals, such as olivine in the upper mantle, sank through magma. At the same time, partly crystalline mush compacted under gravity, expelling melt. The resulting fractional melt would have been komatiitic to basaltic, rather than having the composition of bulk mantle. At reasonable mantle temperatures for the early Hadean, water and CO_2 would not significantly enter the solid phases in the shallow mantle. The bulk of these volatiles thus ended up in the atmosphere, as the mantle had to circulate through shallow depths to cool. In analogy, bubbles escape efficiently from modern volcanoes [51,52] and CO_2 escapes from mid-ocean ridge magma chambers (e.g. [17,53]).

As about an ocean of water was present in the atmosphere, the surface pressures were comparable to those within mid-oceanic hydrothermal systems. Therefore, surface rock–atmosphere reactions also occurred at temperatures comparable to those within such systems.

As the atmosphere cooled from runaway greenhouse conditions, a solid surface lid formed above mostly frozen magma. Elements that were in the gas phase in the runaway atmosphere, as found in the calculations of Lupu *et al*. [4], condensed as the atmosphere cooled. Applying the work of Kvande *et al*. [25], we estimate that NaCl–KCl was the first significant non-silicate liquid to condense by approximately 1275 K. As it cooled, the NaCl fluid became more hydrous, the salty liquid water ocean condensed at approximately 400°C, followed by the start of hydrothermal circulation.

We continue with the properties of the cool lid just after the runaway greenhouse collapsed and the ocean condensed. To provide an example, the surface temperature under 100 bar of CO_2 was approximately 500 K and the interior temperature was 1900 K, and thus the gradient ΔT_{BL} was 1400 K. We can then estimate the thickness of the lid assuming conductive heat transfer. For the runaway greenhouse threshold of 110 W m^{-2}, the corresponding surface boundary-layer thickness Z_{BL} is 32 m. Given a heat flow of 10 W m^{-2}, this results in a 350 m thick lid. These estimates ignore hydrothermal circulation and hence are too small to be credible.

Modern ultrafast ridges illustrate the efficacy of hydrothermal thermal circulation, melt segregation and melt freezing beneath a liquid ocean. Only a thin lens of fully molten magma is present at approximately 0.5 km depth (e.g. [54]). At the axis, the remainder of the crust beneath this lens is nearly solid mush, mostly crystalline. The heat conducted through a thin solid layer just above the magma lens is carried into the ocean by hydrothermal circulation. Heat balance calculations indicate that this heat flow is 30–40 W m^{-2} [44,54]. This value is high enough that hydrothermal convection through the nascent ocean could have been the mechanism responsible for transporting a significant fraction of the critical runaway greenhouse heat flow of 110 W m^{-2} through a global lid above mostly frozen magma.

We qualitatively explain overcooling of the interior mantle during the epoch of a thin cool lid using an analogy with the lava erupting through the lid at ultrafast ridge axes [44,54]. A globally extensive lid would have been even more likely to founder than the lateral narrow lid at ridge axes. In analogy to a lava lake, material would ascend into the lid at spreading centres, diverge laterally and cool, and then founder into the underlying hot material. Lid material once foundered would sink to great depth. Once the available hot mantle material was processed through the surface lid, the bulk mantle would have cooled to a temperature somewhat below that of the hot material. In terms of (4.10), it follows that the whole mantle cycled through the thin lid boundary layer less than once during this entire epoch.

Rapid sinking would have carried lid material to great depths without extensively cooling the intervening hot material beneath the lid. Then, the remaining hot material could continue to ascend into the lid and cool. At the end of this process, the bulk of the hot material would have passed through the lid, foundered and accumulated at depth. The net effect would have been the reduction of the average temperature of the mantle towards that of foundered lid material. In this scenario, radioactivity then heated the Hadean mantle from this minimum state to a maximum in the mid-Archaean [49].

Overall, resolving shallow Hadean events at the end of the runaway greenhouse from mantle samples is not straightforward, as all described processes were similar to Archaean and modern ones.

(b) Samarium–neodymium systems

We review the samarium–neodymium system, as it provides constraints on absolute geologic timing. In general, partial crystallization results in chemical differentiation within the Earth. This leads to moderate differences between the major element composition of the solid and melt. Partition can have stronger effects on trace elements. Elements that partition almost

completely into the solid are called compatible elements. Conversely, incompatible elements partition strongly into the melt. Partition ratios depend on pressure, temperature and the bulk composition of the melt.

The short-lived samarium–neodymium system provides the possibility of resolving such elemental partitioning within the early Earth. The isotope ^{146}Sm decays to ^{142}Nd with a half-life of 68 Myr [55]. Some ^{146}Sm was present at the time of the Moon-forming impact, but then the isotope became extinct over several more half-lives. Therefore, variations in the ratio ^{142}Nd/^{144}Nd, where ^{144}Nd has no significant radiogenic component, could have formed only in the early Hadean. Both Nd and Sm are moderately incompatible rare earth elements. Nd is more incompatible than Sm, but their chemical similarity precludes trace phases from strongly concentrating one of the elements but not the other. Furthermore, the application of this isotopic system to terrestrial processes is simplified in that it was probably not affected significantly by the arrival of extraterrestrial material after the Moon-forming impact.

Within resolution, the ratio ^{142}Nd/^{144}Nd is constant over modern mid-ocean ridge and oceanic island models [56]. The sampled regions are believed to represent most of the silicate Earth. Still, ^{142}Nd/^{144}Nd variations persist within ancient rocks, indicating that some early Hadean Nd–Sm fractionation did occur while ^{146}Sm was still present a few half-lives after the Moon-forming impact. Tectonics subsequently remixed most of the Earth's crust and mantle.

^{142}Nd/^{144}Nd variations have been measured in multiple locations around the world. In particular, Iizuka *et al*. [57] measured ^{142}Nd/^{144}Nd variations in the 3.6–4.1 Ga Acasta Gneiss and approximately 3.8 Ga rocks in Greenland. Rizo *et al*. [58] also discuss Greenland samples. Tessalina *et al*. [59] report ^{142}Nd/^{144}Nd variations in Archaean cherts and lavas that were probably derived at the expense of Hadean crustal rocks. O'Neil *et al*. [60–62] and Adam *et al*. [63] associate ^{142}Nd/^{144}Nd variations in greenstones within the Nuvvuagittuq region of Québec with their early eruption in the Hadean. Alternatively, these rocks may have erupted in the Archaean and formed by partial melting of an early Hadean mantle domain [64]. In the model of Guitreau *et al*. [64], the Hadean domain formed at approximately 4.51 Ga.

We note that the absolute time of the Moon-forming impact is not well constrained, so we cannot provide precise absolute times from ^{142}Nd/^{144}Nd results either. Avice & Marty [65] proposed that the impact occurred 40–50 Myr after the start of the Solar System, or approximately 4.52 Ga, from an analysis of xenon isotopes. Borg *et al*. [66] and Carlson *et al*. [67] note that the earliest reliable lunar age is 4.36 Ga, but prefer a lunar age slightly older than this. Further discussion of the age of the Moon is beyond the scope of this paper. Terrestrial radiometric clocks including those of zircons (e.g. [68,69]) were potentially preserved soon after the Moon-forming impact. Overall, ^{142}Nd variations could tag chemical domains for geochemical studies to infer the post-impact conditions, such as the Earth becoming mostly solid soon after the impact (figure 1).

(c) Freezing of deep mantle

In contrast to shallow-mantle processes, combined studies of multiple isotopic systems currently provide information on igneous processes in the deep mantle following the Moon-forming impact. Partial crystallization at lower mantle depths produced chemically heterogeneous rocks that later remelted and became the source region for basaltic magmas. Rizo *et al*. [58] associate ^{142}Nd/^{144}Nd variations in Archaean lavas with this process. Guitreau *et al*. [64] also discussed the possibility that a mantle source of this type produced ^{142}Nd/^{144}Nd variation within early Archaean lavas from Québec. Jackson & Carlson [56] point out that partial crystallization of the mantle in the early Hadean could have formed 'hidden' low-Sm/Nd reservoirs, leaving the rest of the mantle with Sm/Nd approximately 6% higher than the probable meteorite source of the Earth. Alternatively, they suggest that the Earth may not have accreted the model meteorite composition.

Returning to simple physics, chemical heterogeneities probably formed within the lower mantle as it froze (figure 3). The increase of lithostatic pressure within the Earth had major effects. First, the stable solid-phase assemblage changes with pressure at constant bulk composition. Partial freezing increases the density of the fluid plus solid system, and hence both the liquidus

and the solidus temperatures increase with depth. The temperature along a liquid or solid adiabat also increases with depth [21]. The melting gradient is thus much steeper than the adiabatic gradient in the upper mantle. It is conceivable that this relationship between the adiabat and the melting point continues all the way down to the core–mantle boundary. If so, the mantle froze from bottom up, and in this case tidal dissipation would have been concentrated within the deep region of freezing. Heating from below would have kept the mantle well mixed until tidal heating and the runaway greenhouse collapsed.

On the other hand, it is also conceivable that freezing began within the middle of the lower mantle [35]. In this case, tidal dissipation would have been concentrated initially in the middle of the mantle. Heated material ascended and remelted, but the deeper mantle remained stagnant and isolated from the atmosphere and the upper mantle. Dense melts may have intruded downward, forming deep dreg layers in the mantle that later ascended within plumes [70].

In all cases, the thickness of the partially molten tidal-heating mush zone increased as the Moon retreated to keep the total heat flow at the critical runaway greenhouse threshold. At the end of the hot greenhouse, partially molten convecting slurry would have been present near the surface. However, because melting temperatures increase more rapidly with depth than the adiabats in the upper mantle, the actual geotherm could not have both followed the adiabat, yet also maintained the constant melt fraction that optimizes tidal dissipation. Put another way, the viscosity could not have been both approximately 10^9 Pa s suitable for efficient convection within slurry and approximately 10^{11} Pa s for dissipative mush. Most likely, the deep mantle was mostly solid, the deep upper mantle was mush, while the uppermost mantle was still slurry.

We show some qualitative inferences based on the theory of convection with the goal of finding potentially testable hypotheses with regard to heterogeneous mantle temperatures relative to an adiabat curve. Boundary-layer theory yields a valid estimate of convective heat flow, provided that the thickness of the fluid slurry region was much larger than its boundary layer. The theoretical assumption that the material descending (like slabs on modern Earth) from the surface boundary layer continues to sink does not apply if the viscosity increases too rapidly with depth [39]. Material sinking through liquid and/or slurry mantle would have slowed down when it encountered high-viscosity mush and would have ponded within the even more viscous deep solid mantle. The temperatures of the solid mantle at a given depth would have become heterogeneous when cooler material ponded more in some domains relative to others. Unusually hot mantle would tend to rise, as with modern mantle plumes, and cold material would continue to sink, like modern slabs. Wholesale turnover of the deep mantle may have occurred as it heated while the upper mantle cooled [19].

These processes are important for the petrology of lavas in analogy with modern mantle plumes. They have only modest effects on thermal history calculations, including those in figure 1, which assume an adiabatic mantle for convenience (e.g. [48,49]). Evidence of heterogeneous mantle temperatures is then provided by Archaean igneous rocks, but there are no relevant Hadean data [48–50].

6. From warm greenhouse to habitability

We examine the physics and geochemistry of the transition of Earth to habitability, continuing our effort to present reasonable hypotheses that are potentially testable. Along these lines, we will look for a climatic marker linked to tectonics brought by the advent of habitability on Earth. As a caveat, the physics of modern plates is not well-enough understood to apply it with confidence to the Hadean or to other planets [71].

(a) Biological constraints on Hadean tectonics and climate

It is likely that the ocean condensed under a dense approximately 100 bar CO_2 atmosphere once internal heating fell below the critical runaway greenhouse threshold [6,72]. This is consistent with the initial water and CO_2 composition of our atmospheric models. The surface temperature

under such an atmosphere would have been approximately 200°C, too hot for life as we know it. For reference, the current temperature record for life is 122°C [73]. Earth became habitable once the surface temperature decreased into the range tolerated by thermophile organisms, which implies a CO_2 pressure of approximately 25 bar [72]. The origin of life under thermophile conditions (e.g. [74]) thus remains a viable hypothesis. Going further, a clement environment for life would appear under an approximately 1 bar CO_2 atmosphere.

The Earth appears to have been inhabited as soon as sedimentary rocks appear in the geological record at approximately 3.8 Ga. Thus it is likely that most of the CO_2 was subducted by that time. Abundant evidence of life in highly metamorphosed early Archaean rocks indicates that the process occurred before intact surface rocks appear in the geological record (e.g. [75]). Early Archaean metasediments contain reduced-carbon-rich metamorphic rocks, which probably formed at the expense of biological carbon-rich black shales [76].

Early Archaean banded iron formation was also probably formed by biological processes. Furthermore, it requires a low CO_2 partial pressure. Studies of rare earth elements within these rocks indicate that the early oceanic pH was approximately 8, similar to the modern level [77]. This inference taken at face value indicates that the atmospheric CO_2 partial pressure was no more than a few times the present level. Otherwise, open-ocean iron formation would have been precluded beneath a massive CO_2 atmosphere, because ferrous iron is insoluble in seawater at this pH and approximately 1 bar CO_2. Moreover, early Archaean banded iron formation contains magnetite Fe_3O_4, which is unstable relative to haematite Fe_2O_3 and siderite $FeCO_3$ at high CO_2 pressures [78]. Overall, this evidence indicates that the epoch of the approximately 1 bar CO_2 atmosphere finished before the time when the oldest Archaean sediments formed.

It is therefore inevitable to infer that the Earth passed through clement conditions under an approximately 1 bar CO_2 partial pressure at some time after the Moon-forming impact [72]. Molecular biologists have recognized that this epoch characterized by a massive CO_2 atmosphere was favourable for the origin of life. For example, the Hadean ocean pH was then approximately 6, rather than the modern value of approximately 8, in which case phosphorus and ferrous iron were soluble in water [79]. Nascent life may have used the pH gradient between the ocean (approx. 6) and the serpentine hydrothermal vents (approx. 11) as its energy source [79–82]. In general, molecular biology studies make inferences on the Hadean Earth environment, here that serpentine was present and that the CO_2 pressure was approximately 1 bar. One would also have to reconcile the time constraints extrapolating from known life backwards by approximately 3.8 Ga. The use of molecular clocks in such situations is fraught with difficulty [83].

With regard to the potential pre-biotic environment, we infer that very CO_2-rich and somewhat hydrated oceanic crust would have subducted at the time that the Earth first became habitable. The Hadean arc magmas were probably different from modern arc magmas (see §6*b*), where CO_2 plays a modest role in the subducted crust. The composition of primitive CO_2-rich Hadean arc lavas is presently being characterized through experiments on melting of fully carbonatized basaltic rock at mantle pressure [84,85]. In addition to being rich in CO_2, such magmas were probably rich in alkalis and poor in aluminium. Holm & Baltscheffsky [86] and Holm [87] discussed attractive pre-biotic aspects of such lavas that ascended to shallow clement depths and the surface. Available polymerized phosphate formed as the magmas froze. Brines that formed from water circulation through these solidified rocks was alkaline and reducing. Silicate and borate ions in the solution would stabilize ribose, the building block for RNA. Further discussion of the ascent of these arc magmas and their interactions with the surface environment is beyond the scope of this paper.

(b) Ancient subduction

As stated above, we infer that most of the Earth's CO_2 had entered the mantle before the earliest sedimentary record at approximately 3.8 Ga. There is no obvious alternative crustal reservoir to sequester the CO_2 and no Hadean or early Archaean evidence that one existed. A process with the same net effect as subduction is required. We concentrate on modern

subduction because it is available for study. We briefly discuss alternatives to subduction, before describing geological evidence for ancient subduction, and the physics related to the fate of CO_2 in modern subduction.

Johnson *et al*. [88] proposed a hypothesis for Hadean and early Archaean tectonics that is similar to the behaviour observed on the Jovian satellite Io. In this model, thick sequences of lava flows formed by extensive partial melting and ascended to the surface with minimal fractional crystallization and were thus iron-rich. Each exposed lava flow weathered, forming hydrous minerals and carbonates before being buried by a subsequent flow. Lava beds eventually became buried at approximately 45 km depth. Under this metamorphic condition, the iron-rich lavas became denser than the underlying mantle, and they foundered, carrying CO_2 into the mantle.

We doubt that voluminous flow piles could erupt without fractional crystallization and hence that this mechanism could have transferred globally significant amounts of cold material and CO_2 into the Hadean mantle. This is based on the fact that hot primitive lavas from mantle plumes rarely make it to the surface, while erupted lavas show extensive fractional crystallization. In particular, basalts with extensive fractional crystallization rather than primitive magma are observed to erupt in Iceland and Hawaii.

Two-sided subduction is another conceivable way to deeply subduct CO_2. This putative process requires a brief description, as it does not occur on modern Earth. As two oceanic plates converge and descend, the shallow oceanic crust on both plates will be captured in the middle of the combined descending slab. This crust will remain cold, trapping the CO_2 within. However, this mode of subduction can be excluded on mechanical grounds, as it requires the cool lithosphere of both plates to bend sharply at right angles, while the lithosphere of the oceanic plate bends gradually into the trench with ordinary subduction. Crameri *et al*. [89] confirmed these inferences with numerical calculations.

There is some geological evidence in support of the antiquity of modern subduction. Harrison [68] and Hopkins *et al*. [69] interpreted the record of Hadean zircons preserved within younger sediments to indicate that subduction was taking place at the time. Turner *et al*. [90] note that volcanic rocks near Nuvvuagittuq, Québec, which are at least as old as 3.8 Ga, and possibly older than 4.4 Ga, resemble those from the Izu–Bonin–Mariana forearc (the region between the typical location of volcanoes and the trench). Pons *et al*. [91] showed the similarity between 3.7 and 3.8 Ga serpentines from Isua, Greenland, and modern forearc serpentines.

A potential geochemical tracer of subduction would be the carbonates formed when the ejecta produced by asteroid impacts reacted with the atmospheric CO_2 [92]. This process supplied materials rich in Pt-group elements with carbonates to subduction zones. This mode of CO_2 burial still required extensive geological time and eventual subduction. In addition, dynamic calculations indicate that impactor flux waned after the Moon-forming impact and peaked late in the Hadean at approximately 4.1 Ga [93,94], which would affect the total length of time needed to subduct the CO_2 via this process.

Returning to mechanics, Turner *et al*. [90] also invoked modern subduction to explain their early Archaean rock samples. The thermal aspects of this process are essential to the fate of CO_2 within the oceanic crust. Modern subduction is one-sided in the sense that the oceanic lithosphere descends as the slab. The lithosphere on the arc (or continent) side does not descend. The crust on top of the slab descending into the mantle is heated by conduction from the overlying hot mantle. At these elevated temperatures, metamorphic reactions occur and water- and CO_2-bearing minerals may become unstable. A water- and CO_2-rich fluid ascends from the subducted crust into the hot overlying mantle, lowering its melting point. These hydrous and CO_2-bearing magmas subsequently ascend and erupt at the island arc, with the net effect that much of the subducted water and some of the subducted CO_2 return to the surface, whereas the rest subducts deeply into the mantle.

An outcome of the modern subduction model is that high temperature within the Hadean and Archaean mantle favoured the breakdown of subducted CO_2-bearing minerals (e.g. [18]). We will return to this topic in §6*e* after we have more extensively discussed Hadean tectonics.

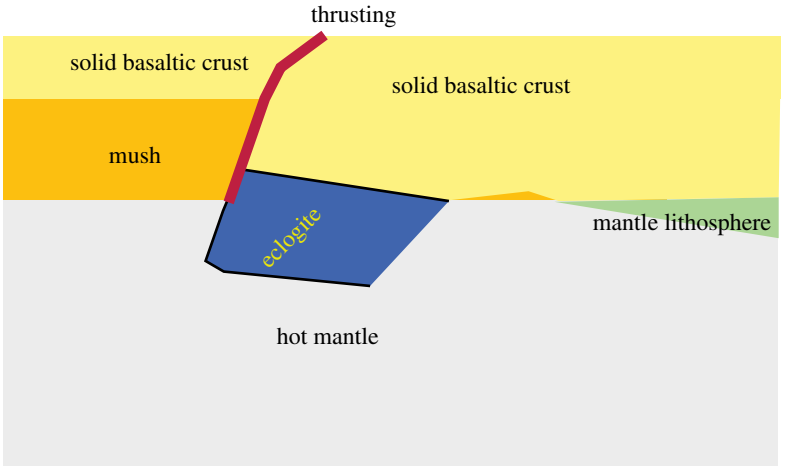

Figure 4. Schematic diagram of gabbroic mush above hot mantle. Slabs of cool basaltic crust sink into the mush. The basalt becomes dense eclogite at depth and sinks into the mantle. This process may have entrained crust above mantle lithosphere and started conventional subduction. (Online version in colour.)

(c) Hadean oceanic crust

Following our inference that habitability on Earth requires CO_2 subduction, we assume for the purposes of discussion that Hadean plate tectonics did occur and begin with a discussion of ridge axes. Basaltic oceanic crust is the product of partial melting of the mantle beneath ridges and is chemically buoyant relative to the mantle at shallow depths. Modern young oceanic lithosphere consists of approximately 6 km thick basaltic crust above a modest thickness of cooled mantle, and thus it does not easily subduct until it is old enough that a thick layer of cooled mantle has developed underneath. The Hadean mantle and certainly the Archaean mantle were hotter than the present mantle. More partial melting must have occurred before being able to subduct, resulting in a thicker oceanic crust. This picture would be analogous to present-day oceanic plateaus, such as Iceland, that formed above hot mantle plumes. These plateaus have a more than 20 km thick crust that does not readily subduct.

The existence of thick oceanic crust and its difficulty to subduct until it is quite old are the classical arguments brought to infer that global Hadean and Archaean plate tectonic rates (in square kilometres of seafloor produced and subducted per year) were lower than the present ones (see [49]). This conclusion does not imply that Hadean subduction was impossible. In §6*d*,*e*, we discuss the roles that gabbroic mush and the transition of basalt to eclogite have played in Hadean subduction.

(d) Non-standard gabbroic mush ocean with plates

The existence of another form of non-standard plate tectonics in the Hadean is conceivable given the Archaean to recent analogues and the geological record [5,44] (figure 4). We have already noted that at modern fast ridge axes mush can cumulate beneath a thin melt lens. Cooled basaltic blocks can then founder into this mush. Translating this hypothesis into the Hadean, partial melting of the ascending mantle could have built up a thick global layer of gabbroic mush beneath the basaltic plates. At mantle plume temperatures and 150 km depths (and hence the temperatures of the Hadean mantle), gabbro transforms into a dense phase assemblage, named eclogite [95]. That is, cold gabbroic crust can sink into hot gabbroic mush, and it can continue to sink into the mantle after it reaches approximately 150 km in depth. However, well above 150 km in depth sinking gabbro does not transform to eclogite and thus cannot continue alone down into the mantle.

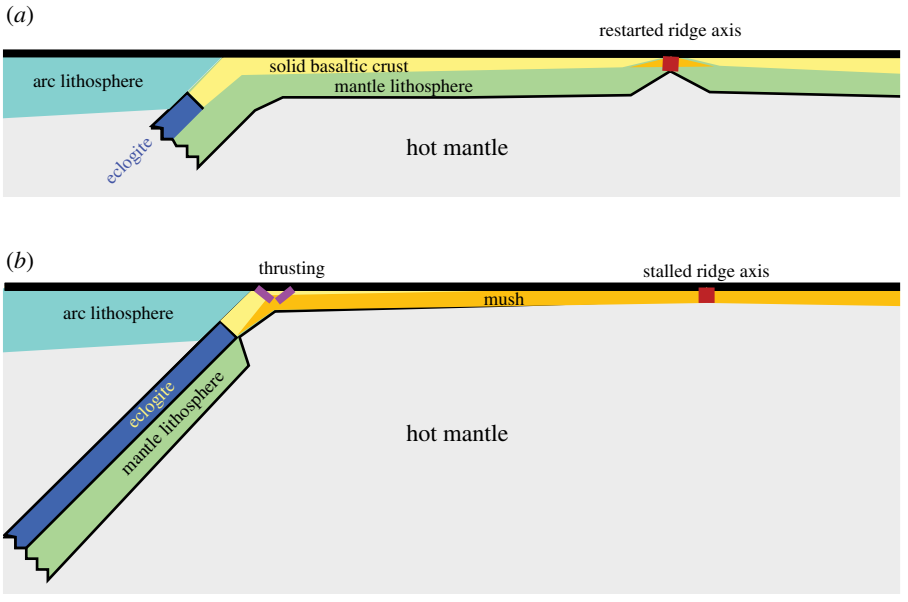

Figure 5. Schematic diagram of Hadean and Archaean plate tectonics. (*a*) Old thick oceanic lithosphere starts to subduct. Eclogite provides driving force. The ridge axis starts to spread rapidly. (*b*) Rapid subduction consumes the old lithosphere. Young lithosphere with buoyant crust jams the subduction zone. The spreading and subduction rates greatly decrease. Basaltic crust locally thrusts into the gabbroic mush. Most of the seafloor was produced at fast ridges and more of the subduction was rapid. Long periods of slow plate motions cause the long-term globally averaged rate of plate motions to be lower than the modern rate. (Online version in colour.)

A stable situation would arise if the mush layer in fact extended down to a depth of approximately 150 km. Cooler gabbro would then sink as eclogite from the mush into the mantle, precluding the depth of the mush layer from getting much deeper than 150 km. The loss of gabbroic mush to eclogite could be balanced by magma input from partial melt. The average mantle temperature now becomes too cold to form a global mush layer 150 km thick. If such a layer did exist, the mantle at some time became too cold to replenish it, the base of the layer moved upwards, with the net result of depleting the mush. Remnants of the depleted mantle and mush layer (including gabbroic slabs) could persist today within the mantle.

Conventional subduction could start after the base of the mush layer became significantly less than 150 km. As they spread away from the ridge axes, gabbroic plates thickened, and well away from the ridge the older lithosphere may have frozen through the mush and cooled into the mantle. A slab made of this lithosphere would have been dense enough to sink through gabbroic mush, and could descend somewhat into the underlying mantle if this mantle was sufficiently cool (figure 4). Once this happened, the gabbro would transform to eclogite and then subduct. This process requires old lithosphere to start.

The available heat budget indicates that Hadean plate velocities were on average low and subducting slabs were typically old [48,49]. However, brief periods of rapid subduction were likely once slabs with thick oceanic crust penetrated to depths of several tens of kilometres, where eclogite is stable at cool slab temperatures (figure 5). The formation of eclogite provided strong negative buoyancy until the subduction zone consumed the available old lithosphere [96]. This phase ended and subduction was greatly slowed when very young lithosphere started to be dragged down. This time was probably characterized by thrusting of oceanic crust into gabbro and low-Ni granite production. As noted by van Hunen & Moyen [97], the tendency of Archaean and Hadean slabs to detach would also lead to episodicity.

Subduction of basaltic crust into gabbroic mush has geochemical consequences that are distinct from those of ordinary subduction of basaltic crust into hot mantle, and can therefore be detected. In both cases, hydrous fluids with CO_2 would escape upwards from the subducted crust into the wedge-shaped region of hot overlying gabbro, lowering the melting temperature and producing magmas. Slab gabbro also directly melted into this hydrous magma. These magmas remained Ni-poor, as they interacted only with basaltic rocks (including the hot gabbro wedge). By contrast, modern and ancient magmas that interacted with the mantle wedge above the slab are Ni-rich.

Studies of nickel concentration show that this local thrusting of cooled hydrous basaltic magma into hot gabbro occurred on a moderate scale in the Archaean. For example, a common subclass of the Archaean TTG suite (trondhjemite, tonalite and granodiorite) of granitic rocks contains little Ni and Cr (which are abundant in the mantle but not in gabbro) (e.g. [98]). Jamaica is also a Cenozoic locality where thrusting occurred within a hot young submarine plateau [99,100].

It is unlikely that hard-to-subduct young oceanic crust would have arrived at the subduction zone all at the same time. Colliding plate boundaries do not fit like jigsaw pieces, especially on a spherical surface. Rather, old easy-to-subduct crust would continue to subduct on a large plate while young crust jammed the rest of the subduction zone. The early Archaean record of forearc volcanism and serpentine intrusion [90,91] bears on this issue. A modern analogy is the Izu–Bonin–Mariana arc, which occurs where the old lithosphere from the very large Pacific plate subducts. Phenomenologically, forearc and backarc spreading allow the slab to subduct rapidly without having the whole Pacific margin subduct rapidly. Conversely, driving forces from old dense slabs lead to convergence along the remainder of the plate boundary, as is the case here with the TTG-forming regions where gabbro sinks into mush.

(e) Hadean CO_2 subduction

We now concentrate on the fate of subducted CO_2 into the mantle. This discussion shuns physical arguments that preclude early Archaean life with the caveat that other Earth-like planets may have behaved differently.

There is no available indication from the rock record of when CO_2 subduction occurred in the Hadean. With regard to putative evidence, Upadhyay *et al*. [101] presented a sample of 3.6 Ga magma derived from a Hadean CO_2-rich mantle source with $^{142}Nd/^{144}Nd$ anomalies. This could have formed only early in the Hadean when the parent isotope ^{146}Sm was extant. However, Roth *et al*. [102] were unable to replicate these $^{142}Nd/^{144}Nd$ measurements.

We present a self-consistent scenario based on the works of Sleep *et al*. [72], Herzberg *et al*. [48,49] and Dasgupta [18] that begins with mass balances and results in subduction. Carbonates of divalent cations are stable at temperatures ranging from warm, approximately 200°C greenhouse conditions down to clement conditions [72]. With regard to kinetics, the reaction of CO_2 with basalt to form carbonate is fast above 1 bar pressure. This is well understood, as the injection of CO_2 into basalt is a candidate process for the industrial sequestration of CO_2 (e.g. [103]).

To remove the required amount of CO_2 from the atmosphere, we invoke ordinary subduction into the mantle, as CO_2 does not significantly enter minerals within gabbroic mush. Let us begin with the available capacity for CO_2 in the oceanic crust. The density of basalt is approximately $3000\,kg\,m^{-3}$, such that the global mass of a 1 km thick layer enveloping the world is thus 1.5×10^{21} kg. CaO, MgO and FeO are abundant in basalt, in round numbers 10% each by mass. In total, there are approximately 30% divalent cation oxides with a mean molecular weight of approximately $0.056\,kg\,mol^{-1}$, giving approximately 0.82×10^{22} mol. Komatiitic crust has similar total concentrations of divalent cations.

The current mantle plus crust reservoir of CO_2 is somewhat greater than 100 bar (1.2×10^{22} mol) [53]. We let 2.5×10^{22} mol [104] be a reasonable upper limit. In this case, the full carbonatization of a global equivalent thickness of 3 km ($2.5/0.82 \approx 3$) of oceanic crust could store the global CO_2 reservoir. However, this amount of carbonatization is unlikely. Hydrothermal circulation at warm near-axis vents carries CO_2 into the oceanic crust, where only the uppermost

crustal layer with a thickness of approximately 0.5 km reacts with the fluid, becoming carbonate. On the inference that Hadean plate tectonics and hence ridges were rapid, Sleep *et al*. [72] concluded that 300 m of accessible crust could accommodate only 0.4×10^{22} mol (32 bar) of CO_2 at any one time.

Young hot Hadean slabs, however, were unlikely to deeply subduct CO_2 [18]. CO_2 is most likely to deeply subduct if the uppermost slab remains cool. This thermal situation occurs with rapid subduction of old oceanic crust at Hadean mantle temperatures [18]. This can only occur kinematically if spreading and subduction rates are episodic, as we inferred in §6*d*. That is, rapid subduction of old crust, once started, required rapid seafloor spreading. The spreading and subduction rates then waned once the young crust arrived at the subduction zone. To summarize, spreading rates were slow most of the time, but rapid spreading rates produced most of the seafloor.

These basic features allow us to make some qualitative inferences. As a caveat, Hadean slab temperatures and mineral phase diagrams, such as those in the work of Dasgupta [18], may be somewhat imprecise. We also note that hydrous fluids such as derived from sedimentary mélange are able to extract solid $CaCO_3$ into solution [105], but it is not evident that this process operated on a large scale in the Hadean or even the early Archaean.

We constrain the time needed for subduction to sequester most of the Earth's CO_2 into the mantle using a mass balance argument. As shown above, only approximately 32 bar of CO_2 could fit into the global oceanic crust at any one time. Subduction and seafloor spreading had to renew the global oceanic crust at least a few times to emplace Earth's more than 100 bar of CO_2 into the mantle. At the present subduction and global spreading rate of approximately $3\,km^2\,yr^{-1}$, the surface of the Earth is replaced every 170 Myr. The global Hadean and Archaean rate could have been less than this [48,49], and therefore deep CO_2 subduction could well have taken much of the Hadean to emplace all CO_2 into the mantle. Considering the approximately 500 Myr of available time and the size (more than 100 bar) of the global CO_2 reservoir, the net CO_2 emplacement rates should have been of the order of tens of bars per 100 Myr. From the detectability perspective, both decarbonatized Hadean crust from young hot slabs and deeply subducted carbonatized crust may persist as mantle domains.

7. Conclusion

The heat available after the Moon-forming impact along with the heat from tidal dissipation could have kept the Earth's interior molten and the atmosphere in a runaway greenhouse state for only approximately 10 Myr. The atmosphere was thick, deep and opaque to thermal radiation, such that the effective temperature of the emitted radiation was comparable to that of the modern Earth, in spite of the hot surface. This atmosphere enforced a cooling rate on the interior of the Earth of the order of $100\,W\,m^{-2}$. This rate of cooling continued until the excess heat was gone and the critical runaway greenhouse state could no longer be maintained. At this point, the water in the atmosphere rained out and accumulated as oceans, leaving 100 bar of CO_2 behind. The resulting surface temperature was of the order of 500 K. In this case as well, the heat escaped to space at effective temperatures comparable to modern ones.

At the end of this process, the upper mantle consisted of partially molten slurry above mostly solid mush, while the deep mantle was probably solid. As recognized by petrologists, during this epoch partial crystallization occurred throughout the mantle, and fractionated elements. Such conditions have never returned. Once present, the solid surface reacted with the atmosphere and then the ocean, and these processes have continued to date. Mantle domains affected by Hadean surface processes have not been recognized as such.

We infer that a process resembling modern subduction sequestered CO_2 into the mantle. The best time constraint for this process is that life existed by approximately 3.8 Ga and that the CO_2 pressure must have decreased to well below 25 bar. Therefore, deep CO_2 subduction probably began soon after the demise of the runaway greenhouse, as Hadean plate tectonics was on average sluggish. Periods of localized rapid subduction and seafloor spreading sent old oceanic crust

into the deep mantle together with much of its CO_2. Given the overall low subduction rate, it is likely that CO_2 was fully emplaced into the mantle only late in the Hadean. Frustratingly to geodynamicists, the best evidence of when the Earth became habitable is still the oldest evidence of life.

Acknowledgements. Jenny Suckale, Dennis Bird and Minik Rosing answered questions. Nils Holm alerted us to his work on phosphate with alkaline magmas. H. J. Melosh and an anonymous reviewer provided helpful comments. This work was performed as part of our collaboration with the NASA Astrobiology Institute Virtual Planetary Laboratory Lead Team.

References

1. Canup RM. 2004 Simulations of a late lunar-forming impact. *Icarus* **168**, 433–456. (doi:10.1016/j.icarus.2003.09.028)
2. Canup RM. 2014 Lunar-forming impacts: processes and alternatives. *Phil. Trans. R. Soc. A* **372**, 20130175. (doi:10.1098/rsta.2013.0175)
3. Asphaug E. 2104 Impact origin of the Moon. *Annu. Rev. Earth Planet. Sci.* **42**, 551–578. (doi:10.1146/annurev-earth-050212-124057)
4. Lupu RE, Zahnle K, Marley MS, Schaefer L, Fegley B, Morley C, Cahoy K, Freedam R, Fortney JJ. 2014 The atmospheres of Earthlike planets after giant impact events. *Astrophys. J.* **784**, 27. (doi:10.1088/0004-637X/784/1/27)
5. Zahnle K, Arndt N, Cockell C, Halliday A, Nisbet E, Selsis F, Sleep NH. 2007 Emergence of a habitable planet. *Space Sci. Rev.* **129**, 35–78. (doi:10.1007/s11214-007-9225-z)
6. Kasting JF, Ackerman TP. 1986 Climatic consequences of very high carbon dioxide levels in the Earth's early atmosphere. *Science* **234**, 1383–1385. (doi:10.1126/science.11539665)
7. Solomatov VS. 2000 Fluid dynamics of a terrestrial magma ocean. In *Origin of the Earth and Moon* (eds RM Canup, K Righter), pp. 323–38. Tucson, AZ: University of Arizona Press.
8. Elkins-Tanton LT. 2012 Magma oceans in the inner Solar System. *Annu. Rev. Earth Planet. Sci.* **40**, 113–139. (doi:10.1146/annurev-earth-042711-105503)
9. Schaefer L, Lodders K, Fegley B. 2012 Vaporization of the Earth: application to exoplanet atmospheres. *Astrophys. J.* **755**, 41–56. (doi:10.1088/0004-637X/755/1/41)
10. Kasting JF, Catling D. 2003 Evolution of a habitable planet. *Annu. Rev. Astron. Astrophys.* **41**, 429–463. (doi:10.1146/annurev.astro.41.071601.170049)
11. Abe Y, Abe-Ouchi A, Sleep NH, Zahnle KJ. 2011 Habitable zone limits for dry planets. *Astrobiology* **11**, 443–460. (doi:10.1089/ast.2010.0545)
12. Goldblatt C, Robinson TD, Zahnle KJ, Crisp D. 2013 Low simulated radiation limit for runaway greenhouse climates. *Nat. Geosci.* **6**, 661–667. (doi:10.1038/ngeo1892)
13. Zahnle KJ. 2006 Earth after the Moon-forming impact. *Geochim. Cosmochim. Acta* **70** (Suppl.), A729. (doi:10.1016/j.gca.2006.06.1311)
14. Elkins-Tanton LT. 2011 Formation of early water oceans on rocky planets. *Astrophys. Space Sci.* **332**, 359–364. (doi:10.1007/s10509-010-0535-3)
15. Hamano K, Abe Y, Genda H. 2013 Emergence of two types of terrestrial planet on solidification of magma ocean. *Nature* **497**, 607–611. (doi:10.1038/nature12163)
16. Claire MW, Sheets J, Cohen M, Ribas I, Meadows VS, Catling DC. 2012 The evolution of solar flux from 0.1 nm to 160 μm: quantitative estimates for planetary studies. *Astrophys. J.* **757**, 95–106. (doi:10.1088/0004-637X/757/1/95)
17. Hirschmann MM. 2012 Magma ocean influence on early atmosphere mass and composition. *Earth Planet. Sci. Lett.* **341–344**, 48–57. (doi:10.1016/j.epsl.2012.06.015)
18. Dasgupta R. 2013 Ingassing, storage, and outgassing of terrestrial carbon through geologic time. *Rev. Mineral. Geochem.* **75**, 183–229. (doi:10.2138/rmg.2013.75.7)
19. Elkins-Tanton LT. 2008 Linked magma ocean solidification and atmospheric growth for Earth and Mars. *Earth Planet. Sci. Lett.* **271**, 181–191. (doi:10.1016/j.epsl.2008.03.062)
20. Drake MJ. 2005 Origin of water in the terrestrial planets. *Meteorit. Planet. Sci.* **40**, 519–527. (doi:10.1111/j.1945-5100.2005.tb00960.x)
21. Andrault D, Bolfan-Casanova N, Lo Nigro G, Bouhifd M, Garbarino G, Mezouar M. 2011 Solidus and liquidus profiles of chondritic mantle: implication for melting of the Earth across its history. *Earth Planet. Sci. Lett.* **304**, 251–259. (doi:10.1016/j.epsl.2011.02.006)
22. Ahrens TJ, O'Keefe JD. 1972 Shock melting and vaporization of lunar rocks and minerals. *Moon* **4**, 214–249. (doi:10.1007/BF00562927)

23. Walter LS, Carron MK. 1964 Vapor pressure and vapor fractionation of silicate melts of tektite composition. *Geochim. Cosmochim. Acta* **28**, 937–951. (doi:10.1016/0016-7037(64)90042-0)
24. Fegley Jr B, Schaefer LK. 2014 Chemistry of Earth's earliest atmosphere. In *Treatise on geochemistry*, 2nd edn (eds HD Holland, KK Turekian), vol. 6, *The atmosphere – history* (ed. J Farquhar), pp. 71-90. Amsterdam, The Netherlands: Elsevier. (doi:10.1016/B978-0-08-095975-7.01303-6)
25. Kvande H, Linga H, Motzfeldt K, Wahlbeck PK. 1979 A thermogravimetric method for determination of vapour pressures above 10^{-2} atm. II. Vapour pressure of molten sodium chloride. *Acta Chem. Scand. A* **33**, 281–288. (doi:10.3891/acta.chem.scand.33a-0281)
26. Canup RM. 2012 Forming a Moon with an Earth-like composition via a giant impact. *Science* **338**, 1052–1055. (doi:10.1126/science.1226073)
27. Ćuk M, Stewart ST. 2012 Making the Moon from a fast-spinning Earth: a giant impact followed by resonant despinning. *Science* **338**, 1047–1052. (doi:10.1126/science.1225542)
28. Magistrale H, Day S, Clayton RW, Graves R. 2000 The SCEC Southern California reference three-dimensional seismic velocity model version 2. *Bull. Seismol. Soc. Am.* **90**, S65–S76. (doi:10.1785/0120000510)
29. Hayashi K, Martin A, Hatayama K, Kobayashi T. 2013 Estimating deep S-wave velocity structure in the Los Angeles Basin using a passive surface-wave method. *Lead. Edge* **32**, 620–626. (doi:10.1190/tle32060620.1)
30. Agrusta R, Arcay D, Tommasi A, Davaille A, Ribe N, Gerya T. 2013 Small-scale convection in a plume-fed low-viscosity layer beneath a moving plate. *Geophys. J. Int.* **194**, 591–610. (doi:10.1093/gji/ggt128)
31. Bullen KE, Bolt BA. 1985 *An introduction to the theory of seismology*, 4th edn. Cambridge, UK: Cambridge University Press.
32. Lamb H. 1932 *Hydrodynamics*. New York, NY: Dover.
33. Olsen KB, Nigbor R, Konno T. 2000 3D viscoelastic wave propagation in the upper Borrego Valley, California, constrained by borehole and surface data. *Bull. Seismol. Soc. Am.* **90**, 134–150. (doi:10.1785/0119990052)
34. Joyner WB. 2000 Strong motion from surface waves in deep sedimentary basins. *Bull. Seismol. Soc. Am.* **90**, S95–S112. (doi:10.1785/0120000505)
35. Mosenfelder JD, Asimow PD, Frost DJ, Rubie DC, Ahrens TJ. 2009 The $MgSiO_3$ system at high pressure: thermodynamic properties of perovskite, post-perovskite, and melt from global inversion of shock and static compression data. *J. Geophys. Res.* **114**, B01203. (doi:10.1029/2008JB005900)
36. Solomatov VS. 1995 Scaling of temperature- and stress-dependent viscosity convection. *Phys. Fluids* **7**, 266–274. (doi:10.1063/1.868624)
37. Solomatov VS, Moresi L-N. 2000 Scaling of time-dependent stagnant lid convection: application to small-scale convection on Earth and other terrestrial planets. *J. Geophys. Res.* **105**, 21 795–21 817. (doi:10.1029/2000JB900197)
38. Solomatov VS. 2007 Magma oceans and primordial mantle differentiation. In *Treatise on geophysics* (ed. G Schubert), vol. 9, *Evolution of the Earth* (ed. DJ Stevenson), pp. 91–119. Amsterdam, The Netherlands: Elsevier. (doi:10.1016/B978-044452748-6.00141-3)
39. Sleep NH. 2011 Seismically observable features of mature stagnant-lid convection at the base of the lithosphere: some scaling relationships. *Geochem. Geophys. Geosyst.* **12**, Q10018. (doi:10.1029/2011GC003760)
40. Stacey FD. 1977 A thermal model of the Earth. *Phys. Earth Planet. Inter.* **15**, 341–348. (doi:10.1016/0031-9201(77)90096-6)
41. Davaille A, Jaupart C. 1993 Thermal convection in lava lakes. *Geophys. Res. Lett.* **20**, 1827–1830. (doi:10.1029/93GL02008)
42. Davaille A, Jaupart C. 1993 Transient high-Rayleigh-number thermal convection with large viscosity variations. *J. Fluid Mech.* **253**, 141–166. (doi:10.1017/S0022112093001740)
43. Davaille A, Jaupart C. 1994 The onset of thermal convection in fluids with temperature-dependent viscosity: application to the oceanic mantle. *J. Geophys. Res.* **99**, 19 853–19 866. (doi:10.1029/94JB01405)
44. Sleep NH. 2007 Plate tectonics through time. In *Treatise on geophysics* (ed. G Schubert), vol. 9, *Evolution of the Earth* (ed. DJ Stevenson), pp. 145–169. Amsterdam, The Netherlands: Elsevier. (doi:10.1016/B978-044452748-6.00143-7)
45. Shaw HR. 1972 Viscosities of magmatic silicate liquids; an empirical method of prediction. *Am. J. Sci.* **272**, 870–893. (doi:10.2475/ajs.272.9.870)

46. Stockstill-Cahill KR, McCoy TJ, Nittler LR, Weider SZ, Hauck II SA. 2012 Magnesium-rich crustal compositions on Mercury: implications for magmatism from petrologic modeling. *J. Geophys. Res.* **117**, E00L15. (doi:10.1029/2012JE004140)
47. Weatherley SM, Katz RF. 2012 Melting and channelized magmatic flow in chemically heterogeneous, upwelling mantle. *Geochem. Geophys. Geosyst.* **13**, Q0AC18. (doi:10.1029/2011GC003989)
48. Herzberg C, Asimow PD, Arndt N, Niu Y, Lesher CM, Fitton JG, Cheadle MJ, Saunders AD. 2007 Temperatures in ambient mantle and plumes: constraints from basalts, picrites and komatiites. *Geochem. Geophys. Geosyst.* **8**, Q02006. (doi:10.1029/2006GC001390)
49. Herzberg C, Condie K, Korenaga J. 2010 Thermal history of the Earth and its petrological expression. *Earth Planet. Sci. Lett.* **292**, 79–88. (doi:10.1016/j.epsl.2010.01.022)
50. Arndt N. 2003 Komatiites, kimberlites, and boninites. *J. Geophys. Res.* **108**, 2293. (doi:10.1029/2002JB002157)
51. Suckale J, Nave J-C, Hager BH. 2010 It takes three to tango: 1. Simulating buoyancy-driven flow in the presence of large viscosity contrasts. *J. Geophys. Res.* **115**, B07409. (doi:10.1029/2009JB006916)
52. Suckale J, Hager BH, Elkins-Tanton LT, Nave J-C. 2010 It takes three to tango: 2. Bubble dynamics in basaltic volcanoes and ramifications for modeling normal strombolian activity. *J. Geophys. Res.* **115**, B07410. (doi:10.1029/2009JB006917)
53. Hirschmann MM, Dasgupta R. 2009 The H/C ratios of Earth's near surface and deep reservoirs, and the consequences for deep Earth volatile cycles. *Chem. Geol.* **262**, 4–16. (doi:10.1016/j.chemgeo.2009.02.008)
54. Fontaine FJ, Olive J-A, Cannat M, Escartin J, Perol T. 2011 Hydrothermally induced melt lens cooling and segmentation along the axis of fast and intermediate-spreading centers. *Geophys. Res. Lett.* **38**, L14307. (doi:10.1029/2011GL047798)
55. Kinoshita N *et al*. 2012 A shorter ^{146}Sm half-life measured and implications for ^{146}Sm–^{142}Nd chronology in the Solar System. *Science* **335**, 1614–1617. (doi:10.1126/science.1215510)
56. Jackson MG, Carlson RW. 2012 Homogeneous superchondritic ^{142}Nd/^{144}Nd in the mid-ocean ridge basalt and ocean island basalt mantle. *Geochem. Geophys. Geosyst.* **13**, Q06011. (doi:10.1029/2012GC004114)
57. Iizuka T, Nakai S, Sahoo YV, Takamasa A, Hirata T, Maruyama S. 2010 The tungsten isotopic composition of Eoarchean rocks: implications for early silicate differentiation and core–mantle interaction on Earth. *Earth Planet. Sci. Lett.* **291**, 189–200. (doi:10.1016/j.epsl.2010.01.012)
58. Rizo H, Boyet M, Blichert-Toft J, Rosing M. 2011 Combined Nd and Hf isotope evidence for deep-seated source of Isua lavas. *Earth Planet. Sci. Lett.* **312**, 267–279. (doi:10.1016/j.epsl.2011.10.014)
59. Tessalina SG, Bourdon B, Kranendonk M, Birck JL, Philippot P. 2010 Influence of Hadean crust evident in basalts and cherts from the Pilbara Craton. *Nat. Geosci.* **3**, 214–217. (doi:10.1038/ngeo772)
60. O'Neil J, Carlson RW, Francis D, Stevenson RK. 2008 Neodymium-142 evidence for Hadean mafic crust. *Science* **321**, 1828–1831. (doi:10.1126/science.1161925)
61. O'Neil J, Francis D, Carlson RW. 2011 Implications of the Nuvvuagittuq Greenstone Belt for the formation of Earth's early crust. *J. Petrol.* **52**, 985–1009. (doi:10.1093/petrology/egr014)
62. O'Neil J, Carlson RW, Paquette J-L, Francis D. 2012 Formation age and metamorphic history of the Nuvvuagittuq Greenstone Belt. *Precambrian Res.* **220–221**, 23–44. (doi:10.1016/j.precamres.2012.07.009)
63. Adam J, Rushmer T, O'Neil J, Francis D. 2012 Hadean greenstones from the Nuvvuagittuq fold belt and the origin of the Earth's early continental crust. *Geology* **40**, 363–366. (doi:10.1130/G32623.1)
64. Guitreau M, Blichert-Toft J, Mojzsis SJ, Roth ASG, Bourdon B. 2013 A legacy of Hadean silicate differentiation inferred from Hf isotopes in Eoarchean rocks of the Nuvvuagittuq supracrustal belt (Québec, Canada). *Earth Planet. Sci. Lett.* **362**, 171–181. (doi:10.1016/j.epsl.2012.11.055)
65. Avice G, Marty B. 2014 The iodine–plutonium–xenon age of the Moon–Earth system revisited. *Phil. Trans. R. Soc. A* **372**, 20130260. (doi:10.1098/rsta.2013.0260)
66. Borg LE, Connelly JN, Boyet M, Carlson RW. 2011 Chronological evidence that the Moon is either young or did not have a global magma ocean. *Nature* **477**, 70–73. (doi:10.1038/nature10328)

67. Carlson RW, Borg LE, Gaffney AM, Boyet M. 2014 Rb–Sr, Sm–Nd and Lu–Hf isotope systematics of the lunar Mg-suite: the age of the lunar crust and its relation to the time of Moon formation. *Phil. Trans. R. Soc. A* **372**, 20130246. (doi:10.1098/rsta.2013.0246)
68. Harrison TM. 2009 The Hadean crust: evidence from >4 Ga zircons. *Annu. Rev. Earth Planet. Sci.* **37**, 479–505. (doi:10.1146/annurev.earth.031208.100151)
69. Hopkins MD, Harrison TM, Manning CE. 2010 Constraints on Hadean geodynamics from mineral inclusions in >4 Ga zircons. *Earth Planet. Sci. Lett.* **298**, 367–376. (doi:10.1016/j.epsl.2010.08.010)
70. Wang X-C, Li ZX, Li X-H. 2013 Early differentiation of the bulk silicate Earth as recorded by the oldest mantle reservoir. *Precambrian Res.* **238**, 52–62. (doi:10.1016/j.precamres.2013.09.010)
71. Lenardic A, Crowley JW. 2012 On the notion of well-defined tectonic regimes for terrestrial planets in this solar system and others. *Astrophys. J.* **755**, 132. (doi:10.1088/0004-637X/755/2/132)
72. Sleep NH, Zahnle K, Neuhoff PS. 2001 Initiation of clement surface conditions on the early Earth. *Proc. Natl Acad. Sci. USA* **98**, 3666–3672. (doi:10.1073/pnas.071045698)
73. Takai K *et al*. 2008 Cell proliferation at 122°C and isotopically heavy CH_4 production by a hyperthermophilic methanogen under high-pressure cultivation. *Proc. Natl Acad. Sci. USA* **105**, 10 949–10 954. (doi:10.1073/pnas.0712334105)
74. Pace NR. 1991 Origin of life: facing up to the physical. *Cell* **65**, 531–533. (doi:10.1016/0092-8674(91)90082-A)
75. Sleep NH, Bird DK. 2007 Niches of the pre-photosynthetic biosphere and geologic preservation of Earth's earliest ecology. *Geobiology* **5**, 101–117. (doi:10.1111/j.1472-4669.2007.00105.x)
76. Ohtomo Y, Kakegawa T, Ishida A, Nagase T, Rosing MT. 2014 Evidence for biogenic graphite in early Archaean Isua metasedimentary rocks. *Nat. Geosci.* **7**, 25–28. (doi:10.1038/ngeo2025)
77. Friend CRL, Nutman AP, Bennett VC, Norman MD. 2008 Seawater-like trace element signatures (REE + Y) of Eoarchaean chemical sedimentary rocks from southern West Greenland, and their corruption during high-grade metamorphism. *Contrib. Mineral. Petrol.* **155**, 229–246. (doi:10.1007/s00410-007-0239-z)
78. Rosing MT, Bird DK, Sleep NH, Bjerrum CJ. 2010 No climate paradox under the faint early Sun. *Nature* **464**, 744–747. (doi:10.1038/nature08955)
79. Russell MJ, Hall AJ, Martin W. 2010 Serpentinization as a source of energy at the origin of life. *Geobiology* **8**, 355–371. (doi:10.1111/j.1472-4669.2010.00249.x)
80. Nitschke W, Russell MJ. 2009 Hydrothermal focusing of chemical and chemiosmotic energy, supported by delivery of catalytic Fe, Ni, Mo/W, Co, S and Se, forced life to emerge. *J. Mol. Evol.* **69**, 481–496. (doi:10.1007/s00239-009-9289-3)
81. Lane N, Allen JF, Martin W. 2010 How did LUCA make a living? Chemiosmosis in the origin of life. *BioEssays* **32**, 271–280. (doi:10.1002/bies.200900131)
82. Russell MJ, Nitschke W, Branscomb E. 2013 The inevitable journey to being. *Phil. Trans. R. Soc. B* **368**, 20120254. (doi:10.1098/rstb.2012.0254)
83. Graur D, Martin W. 2004 Reading the entrails of chickens: molecular timescales of evolution and the illusion of precision. *Trends Genet.* **20**, 80–86. (doi:10.1016/j.tig.2003.12.003)
84. Kiseeva ES, Yaxley GM, Hermann J, Litasov KD, Rosenthal A, Kamenetsky VS. 2012 An experimental study of carbonated eclogite at 3.5–5.5 GPa—implications for silicate and carbonate metasomatism in the cratonic mantle. *J. Petrol.* **53**, 727–759. (doi:10.1093/petrology/egr078)
85. Kiseeva ES, Litosov KD, Yaxley GM, Ohtani E, Kamenetsky VS. 2013 Melting and phase relations of carbonated eclogite at 9–21 GPa and the petrogenesis of alkali-rich melts in the deep mantle. *J. Petrol.* **54**, 1555–1583. (doi:10.1093/petrology/egt023)
86. Holm NG, Baltscheffsky H. 2011 Links between hydrothermal environments, pyrophosphate, Na^+, and early evolution. *Orig. Life Evol. Biosph.* **41**, 483–493. (doi:10.1007/s11084-011-9235-4)
87. Holm NG. 2014 Glasses as sources of condensed phosphates on the early Earth. *Geochem. Trans.* **15**, 8. (doi:10.1186/1467-4866-15-8)
88. Johnson TE, Brown M, Kaus BJP, Van Tongeren J. 2014 Delamination and recycling of Archaean crust caused by gravitational instabilities. *Nat. Geosci.* **7**, 47–52. (doi:10.1038/ngeo2019)

89. Crameri F, Tackley PJ, Meilick I, Gerya TV, Kaus BJP. 2012 A free plate surface and weak oceanic crust produce single-sided subduction on Earth. *Geophys. Res. Lett.* **39**, L03306. (doi:10.1029/2011GL050046)
90. Turner S, Rushmer T, Reagan M, Moyen JM. 2014 Heading down early on? Start of subduction on Earth. *Geology* **42**, 139–142. (doi:10.1130/G34886.1)
91. Pons M-L, Quitté G, Fujii T, Rosing MT, Reynard B, Moynierd F, Doucheta C, Albarède F. 2011 Early Archean serpentine mud volcanoes at Isua, Greenland, as a niche for early life. *Proc. Natl Acad. Sci. USA* **108**, 17 639–17 643. (doi:10.1073/pnas.1108061108)
92. Sleep NH, Zahnle K. 2001 Carbon dioxide cycling and implications for climate on ancient Earth. *J. Geophys. Res.* **106**, 1373–1399. (doi:10.1029/2000JE001247)
93. Ćuk M. 2012 Chronology and sources of lunar impact bombardment. *Icarus* **218**, 69–79. (doi:10.1016/j.icarus.2011.11.031)
94. Morbidelli A, Marchi S, Bottke WF, Kring DA. 2012 A sawtooth-like timeline for the first billion years of lunar bombardment. *Earth Planet. Sci. Lett.* **355–356**, 144–151. (doi:10.1016/j.epsl.2012.07.037)
95. Sobolev AV, Hofmann AW, Sobolev SV, Nikogosian IK. 2005 An olivine-free mantle source of Hawaiian shield basalts. *Nature* **434**, 590–597. (doi:10.1038/nature03411)
96. Sleep NH, Windley BF. 1982 Archean plate tectonics: constraints and inferences. *J. Geol.* **90**, 363–379. (doi:10.1086/628691)
97. van Hunen J, Moyen J-F. 2012 Archean subduction: fact or fiction? *Annu. Rev. Earth Planet. Sci.* **40**, 195–219. (doi:10.1146/annurev-earth-042711-105255)
98. Hoffmann JE, Münker C, Næraa T, Rosing MT, Herwartz D, Garbe-Schönberg D, Svahnberg H. 2011 Mechanisms of Archean crust formation inferred from high-precision HFSE systematics in TTGs. *Geochim. Cosmochim. Acta* **75**, 4157–4178. (doi:10.1016/j.gca.2011.04.027)
99. Hastie AR, Kerr AC, McDonald I, Mitchell JF, Pearce JA, Millar IL, Barfod D, Mark DF. 2010 Geochronology, geochemistry and petrogenesis of rhyodacite lavas in eastern Jamaica: a new adakite subgroup analogous to early Archaean continental crust? *Chem. Geol.* **276**, 344–359. (doi:10.1016/j.chemgeo.2010.07.002)
100. Hastie AR, Kerr AC, McDonald I, Mitchell JF, Pearce JA, Wolstencroft M, Millar IL. 2010 Do Cenozoic analogues support a plate tectonic origin for Earth's earliest continental crust? *Geology* **38**, 495–498. (doi:10.1130/G30778.1)
101. Upadhyay D, Scherer EE, Mezger K. 2009 ^{142}Nd evidence for an enriched Hadean reservoir in cratonic roots. *Nature* **459**, 1118–1121. (doi:10.1038/nature08089)
102. Roth ASG, Bourdon B, Mojzsis SJ, Touboul M, Sprung P, Guitreau M, Blichert-Toft J. 2013 Inherited ^{142}Nd anomalies in Eoarchean protoliths. *Earth Planet. Sci. Lett.* **361**, 50–57. (doi:10.1016/j.epsl.2012.11.023)
103. Matter JM, Takahashi T, Goldberg D. 2007 Experimental evaluation of in situ CO_2–water–rock reactions during CO_2 injection in basaltic rocks: implications for geological CO_2 sequestration. *Geochem. Geophys. Geosyst.* **8**, Q02001. (doi:10.1029/2006GC001427)
104. Zhang Y, Zindler A. 1993 Distribution and evolution of carbon and nitrogen in Earth. *Earth Planet. Sci. Lett.* **117**, 331–345. (doi:10.1016/0012-821X(93)90088-Q)
105. Ague JJ, Nicolescu S. 2014 Carbon dioxide released from subduction zones by fluid-mediated reactions. *Nat. Geosci.* **7**, 355–360. (doi:10.1038/ngeo2143)